EUROPEAN COMMISSION
5th EURATOM FRAMEWORK PROGRAMME 1998-2002
KEY ACTION : NUCLEAR FISSION

HTR-E

# High-Temperature Reactor Components and Systems

**CONTRACT N°**
**FIKI-CT-2001-00177**

## Delivery D26 – WP 3
## Magnetic and Structural Analyses

J.H. Fokkens

Nuclear Research and consultancy Group

The Netherlands

Dissemination level : RE
Document N°: HTR-E 05/12 D-3-2-2
Status : Final
Deliverable D26

**This page is intentionally left blank**

**Confidential**

# HTR-E WP 3
# Magnetic and Structural Analyses

J.H. Fokkens

Petten, 24 February 2006

20793/05.70431/C

Under the contract of the European Commission and the Netherlands Ministry of Economic Affairs

| | | | |
|---|---|---|---|
| author : | J.H. Fokkens | reviewed : | J.M. Church |
| 37 page(s) | | approved : | V.A. Wichers |

## Acknowledgement

The work reported is carried out for the 5th Framework Programme HTR-E (contract nr. FIKI-CT-2001-00177) with financial support from the European Commision and the Netherlands Ministry of Economic Affairs. The report is a deliverable of NRG to HTR-E WP 3.

## Contents

## List of Tables



## List of Figures

# 1 Introduction

This report contributes to the $5^{th}$ Framework Programme HTR-E WP 3. The aim of this work package is to give an insight in the feasibility of the design of the GT-MHR rotor shaft assembly. The report summarizes the results of the finite element magnetic and structural calculations performed for the proposed design of the axial magnetic bearing for the GT-MHR rotor shaft assembly.

Under normal operation conditions the GT-MHR rotor shaft is supported by Active Magnetic Bearings (AMBs). AMBs do not require lubrication and the stiffnesses of the bearings can be changed during operation by the control system to counter irregularities in the rotation of the rotor shaft.

In [1] it is stated that the design of the radial AMBs for the GT-MHR rotor shaft assembly is feasible. Radial AMBs of this size and load bearing capacity have already been built. Due to the vertical arrangement of the GT-MHR rotor shaft the load bearing capacity of the axial AMB has to be much larger than as for normal size axial AMBs. The design of the axial AMB for the GT-MHR rotor shaft assembly is limited by the maximum diameter of the disk that can be built. In [1] a feasible design for the axial AMB is proposed. However, a single disk design for the AMB has not sufficient load bearing capacity. For the GT-MHR rotor shaft assembly a double disk design will be required to obtain sufficient load bearing capacity.

In this report the load bearing capacities of a single and double disk design for the axial AMB of the GT-MHR rotor shaft assembly are investigated. The load capacities of the axial AMBs designs are calculated using finite element magnetostatic analyses. The stress loads in the bearing disks are calculated using finite element structural analyses.

## 2 Problem Definition

In the GT-MHR design for a high temperature gas-cooled reactor the generator, turbine, and compressors are mounted on a single vertically arranged rotor shaft. Figure 1 shows the layout of the rotor shaft. Under normal operating conditions the rotor shaft is supported by 6 radial and 1 axial Active Magnetic Bearings (AMBs). The axial AMB has to carry the weight of the rotor shaft assembly and compensate the axial forces exerted by the turbine and the HP and LP compressor during operation.

The feasibility of the GT-MHR rotor shaft design is mainly determined by the fact whether the design of the axial Active Magnetic Bearing is feasible. The design of the axial AMB for the GT-MHR rotor shaft assembly is limited by the maximum diameter of the disk, that can be manufactured. In [1] a feasible design for the axial AMB is proposed. The proposed design does not meet the requirements regarding the maximum diameter (1610 mm) specified in [2]. To achieve the required load bearing the diameter of the disk has been increased to the largest disk diameter, that can be manufactured (1800 mm). Despite the increase in disk diameter the design still has not sufficient reserve load capacity. A double disk design is envisaged to have sufficient load bearing capacity under all circumstances.

With the use of finite element analyses the load bearing capacity of the double disk design is investigated. First the load bearing capacity of the single disk design (Figure 2) is calculated using finite element analyses. These calculated results are compared with the results given in [1] as a verification of the utilized model and calculation method.

Secondly, the load bearing capacity of a single disk design with upward and downward lifting capacity (Figure 3) is investigated. In [1] it has been assumed that the vertical force from the rotor shaft was always directed downward, thus the axial AMB only required an upward lifting capacity. During an accident situation the vertical force of the rotor shaft can be directed upward as a results of aerodynamic forces acting on the turbine and the compressors. Therefore, the axial AMB should be able to support downward and upward rotor loads.

In the next step the load bearing capacity of a double disk design (Figure 4) is investigated. The double disk design is also capable of supporting downward and upward rotor loads. Finally, the structural behaviour of a disk under the centrifugal and magnetic loads is investigated.

# 3 Approach

The load bearing capacities of the three axial AMB designs have been determined with the use of magnetostatic finite element analyses. The disk mechanical behaviour has been determined using a static structural finite element analysis. These finite element calculations have been performed using the general purpose finite element code MSC.Marc version 2003 [3].

## 3.1 Geometry and Finite Element Model

Schematic views of the three investigated axial AMBs are shown in the Figures 2, 3, and 4. A detailed view of the modelled geometry for design I is shown in Figure 6. The utilized finite element base model for design I and II is shown in Figure 5. This base model doubled in the axial direction forms the finite element model for design III. The base model consists of 4649 elements and 4915 nodal points. For the magnetostatic and structural analyses the same finite element models have been utilized. For the magnetostatic analyses MARC element type 40 has been used [3]. This element type is an axisymmetric bilinear quadrilateral element with thermal and magnetostatic capabilities. MARC element type 10 has been used for the structural analyses [3]. This element type is an arbitrary quadrilateral ring element.

## 3.2 Material Properties

For the magnetostatic analyses the relative magnetic permeability has to be specified for all materials (Figure 6). The values used for the various components are listed below. For the stator material the actual measured *B-H* relation is used, which has been supplied to NRG in confidence.

| | | |
|---|---|---|
| stator material | : | *B-H* relation |
| ferromagnetic materials | : | $\mu_r = 1000$ |
| non ferromagnetic materials | : | $\mu_r = 1$ |

In the structural analysis linear elastic material behaviour has been assumed for the rotor shaft and disk. For the density, Young's modulus, and Poisson ratio the following values have been applied:

| | | | |
|---|---|---|---|
| $\rho$ | = | 7800 | $kg/m^3$ |
| E | = | 210000 | MPa |
| $\nu$ | = | 0.3 | - |

For the remaining components low values for the density and Young's modulus have been chosen. In this way these components are deactivated in the structural analysis.

## 3.3 Boundary Conditions

In the magnetostatic analyses only a boundary condition is applied at the symmetry axis. At the symmetry axis the magnetic potential is prescribed as zero.

In the structural analyses the radial displacements at the symmetry axis are suppressed. To suppress the rigid body motion of the model the lowest node on the symmetry axis is also suppress in axial direction.

### 3.4 Loading Conditions

For the magnetostatic analyses the electric current through the coils is applied as a loading. Each coil consists of 134 winding turns. The electric current through one winding turn is 15, 30, 45, or 60 Ampères. Thus, the total electric current going through a coil is 2010, 4020, 6030, or 8040 Ampères-turns. The electric current through the coils is applied with alternately a positive and negative sign in the model.

In the structural analysis the disk of the AMB design is loaded by a centrifugal load and the magnetic forces. For the calculation of the centrifugal load the rotational speed of the rotor shaft has to be specified:

$$\omega = 50 \cdot 2 \cdot \pi = 314.159$$

The magnetic or Maxwell forces (in the air gaps) are calculated from the magnetic induction calculated with the magnetostatic analyses according to the following relations:

$$\{F_{\mathrm{MX}}\} = \frac{1}{\mu_0} \cdot \int_s \begin{bmatrix} T_{11} & T_{12} \\ T_{21} & T_{22} \end{bmatrix} \cdot \begin{bmatrix} n_1 \\ n_2 \end{bmatrix} ds \tag{1}$$

where:

$$T_{11} = \frac{1}{2} \cdot B_{\mathrm{x}}^2 - \frac{1}{2} \cdot B_{\mathrm{y}}^2 \tag{2}$$

$$T_{12} = B_{\mathrm{x}} \cdot B_{\mathrm{y}} \tag{3}$$

$$T_{21} = B_{\mathrm{x}} \cdot B_{\mathrm{y}} \tag{4}$$

$$T_{22} = \frac{1}{2} \cdot B_{\mathrm{y}}^2 - \frac{1}{2} \cdot B_{\mathrm{x}}^2 \tag{5}$$

and:

| | | |
|---|---|---|
| $B_{\mathrm{i}}$ | : | magnetic flux density |
| $F_{\mathrm{MX}}$ | : | Maxwell force |
| $n_{\mathrm{i}}$ | : | normal vector |
| $T_{\mathrm{ij}}$ | : | magnetic induction |
| $\mu_0$ | : | magnetic permeability constant |

# 4 Results

## 4.1 Results Magnetostatic Analysis for AMB Design I

The results of the magnetostatic analyses performed for the AMB design given in [1] are given in the Figures 7 to 14. Figure 7 shows the applied electric current. The nominal current is 60 A per turn. With 134 turns per coil the total current through a coil is 8040 At. In adjacent coils the direction of the current is opposite. The magnetic potential distribution is shown in Figure 8. Figure 9 shows the magnetic field intensity in the air gap between the stator and the disk. Figure 10 shows the vector plot of the distribution of the magnetic induction.

The magnetic induction in the gap between the stator and the disk is shown in Figure 11. The resulting magnetic forces on the disk are shown in Figure 12. The total magnetic force acting on the disk is 838 kN. The calculated total magnetic force is smaller than the minimum required magnetic force (1090 kN) given in [1]. This difference in result can be explained by the utilized modelling.

Before the AMB Designs II and III were investigated the differences in result between the performed finite element calculation and the result given in [1] has been investigated in more detail. The air gap induction and the magnetic force have been calculated for various nominal current per turn scenarios. Figure 13 shows the magnetic induction in the air gap as a function of the applied electrical current. The magnetic force as a function of the magnetic current is shown in Figure 14. For the comparison of the results calculated with the finite element model and given in [1] the results are summarized in Table 1. For the maximum induction in the air gap there is a good accordance between the results calculated and presented in [1]. The total magnetic force is in all cases underestimated with the finite element calculation. The total force calculated is strongly influenced by the modelling of the stator around the coils. In the finite element model utilized the stator has not been modelled with sufficient detail accuracy around the coils and gap. This information was not available in [1]. However, the finite element model is considered sufficiently accurate for the investigation performed and presented in this report.

table 1 Magnetic analyses - Comparison of results

| **Electrical current** [ A ] | **Air gap induction** [ T ] | | **Force** [ kN ] | |
|---|---|---|---|---|
| | S2M | FEM | S2M | FEM |
| 15 | 0.44 | 0.47 | 95 | 67 |
| 30 | 0.88 | 0.94 | 372 | 266 |
| 45 | 1.28 | 1.26 | 788 | 553 |
| 60 | 1.56 | 1.41 | 1090 | 838 |

## 4.2 Results Magnetostatic Analysis for AMB Design II

The results of the magnetostatic analyses performed for the AMB design II are given in the Figures 15 to 26. Figures 15 and 16 show the applied electric currents in lift and pull mode. The total current through a coil is 8040 At. The magnetic potential distribution is shown in the Figures 17 and 18. Figures 19 and 20 show the magnetic field intensity in the air gap between the stator and the disk in lift and pull mode respectively. The Figures 21 and 22 show the vector plot of the distribution of the magnetic induction.

The magnetic induction in the gap between the stator and the disk is shown in the Figures 23 and 24.

The resulting magnetic forces on the disk in lift and pull mode are shown in the Figures 25 and 26. The total magnetic force acting on the disk in lift mode is 837 kN. The addition of the extra coils beneath the disk has no influence on the load bearing capacity. The total magnetic force acting on the disk in pull mode is 366 kN. This is sufficient for the vertical force acting on the rotor shaft during an accident situation.

### 4.3 Results Magnetostatic Analysis for AMB Design III

The results of the magnetostatic analyses performed for the double disk AMB design are given in the Figures 27 to 38. Figures 27 and 28 show the applied electric current in lift and pull mode. In lift mode 8 coils are activated and in pull mode 2 coils. The total current through a coil is 8040 At. The magnetic potential distribution in lift and pull mode is shown in the Figures 29 and 30 respectively. Figures 19 and 20 show the magnetic field intensity in the air gap between the stator and the disks in lift and pull mode. The Figures 33 and 34 show the vector plot of the distribution of the magnetic induction in lift and pull mode.

The magnetic induction in the gaps between the stators and the disks is shown in the Figures 35 and 36. There is no difference between the upper and lower disk. The resulting magnetic forces on the disks in lift and pull mode are shown in the Figures 37 and 38. The total magnetic force acting in lift mode is 1674 kN. The total magnetic force acting in pull mode is 366 kN. From these results it can be concluded that a double disk design will have sufficient load bearing capacity to support the vertical rotor shaft of the GT-MHR reactor design.

### 4.4 Results Structural Analysis

Structurally, the most loaded component of an axial AMB is the disk. The disk is loaded by the centrifugal load and the magnetic forces. By means of a finite element analysis the stress levels in the disk due to these loads are calculated. The magnetic force applied is the magnetic lift force calculated with the magnetostatic analysis.

Figure 39 shows the distribution of the radial stress in the disk due to the centrifugal load only. The maximum radial stress level is approximately 260 MPa. The distribution of the Von Mises stress due to the centrifugal load only is shown in Figure 40. The maximum Von Mises stress level is approximately 238 MPa. The highest stresses due to the centrifugal loading occur at the root of the disk.

The distribution of the radial and Von Mises stress as due to the magnetic lift load only are shown in the Figures 41 and 42 respectively. The magnetic lift load results in a bending of the disk. The maximum radial stress level is approximately 44 MPa and the maximum Von Mises stress is approximately 38 MPa. The highest stresses due to the magnetic lift load occur also at the root of the disk.

Figures 43 and 44 show the distribution of the radial and Von Mises stress due to the combined centrifugal and magnetic lift load. the maximum radial and Von Mises stress levels are approximately 304 and 275 MPa respectively. The calculated stress levels compare well with the stress levels given in [1], which are considered the maximum stress levels to be allowed. The centrifugal load is the most severe loading for the disk. It should also be kept in mind that an increase of the rotor speed from 3000 to 3600 rpm will result in an increase of the stresses due to only the centrifugal load with nearly 45%.

## 5 Summary and Conclusions

In this report the load bearing capacities of a single and double disk design for the axial AMB of the GT-MHR rotor shaft assembly have been investigated. Magnetostatic and structural finite element analyses have been performed to determine the magnetic lift forces and the stress loads in the disk.

It can be concluded that a double disk design, as proposed in [1], will have sufficient load bearing capacity for the vertical GT-MHR rotor shaft assembly. However, application of a double disk design will increase the length and complexity of the vertical GT-MHR rotor shaft assembly. It should also be kept in mind that the proposed AMB disk results in an increase of the diameter of the vessel containing the rotor shaft assembly compared to the requirements given in [2].

For the detailed engineering of the double disk axial AMB design further investigations are necessary. Especially regarding the required coupling and the dynamic stability of the rotor shaft assembly with increased length. Before this is done it has first to be determined, whether the vertical rotor shaft assembly with a double disk axial AMB is the best solution for the GT-MHR rotor shaft assembly.

## References

[1] L. Baudelocque. *HTR-E Magnetic bearing - Concept proposal*. Societé de Mecanique Magnetique, Ref. BU1 214/02 rev B, 2-10-2002.

[2] F. Cellier. *WP3 Magnetic bearings and catcher bearings - Functional requirements*. Framatome ANP, Document N$^{o}$: HTR-E-02/06-D-3-1-1, November 2002.

[3] MARC2003 Users manual. *MSC Software Inc.*

## Figures

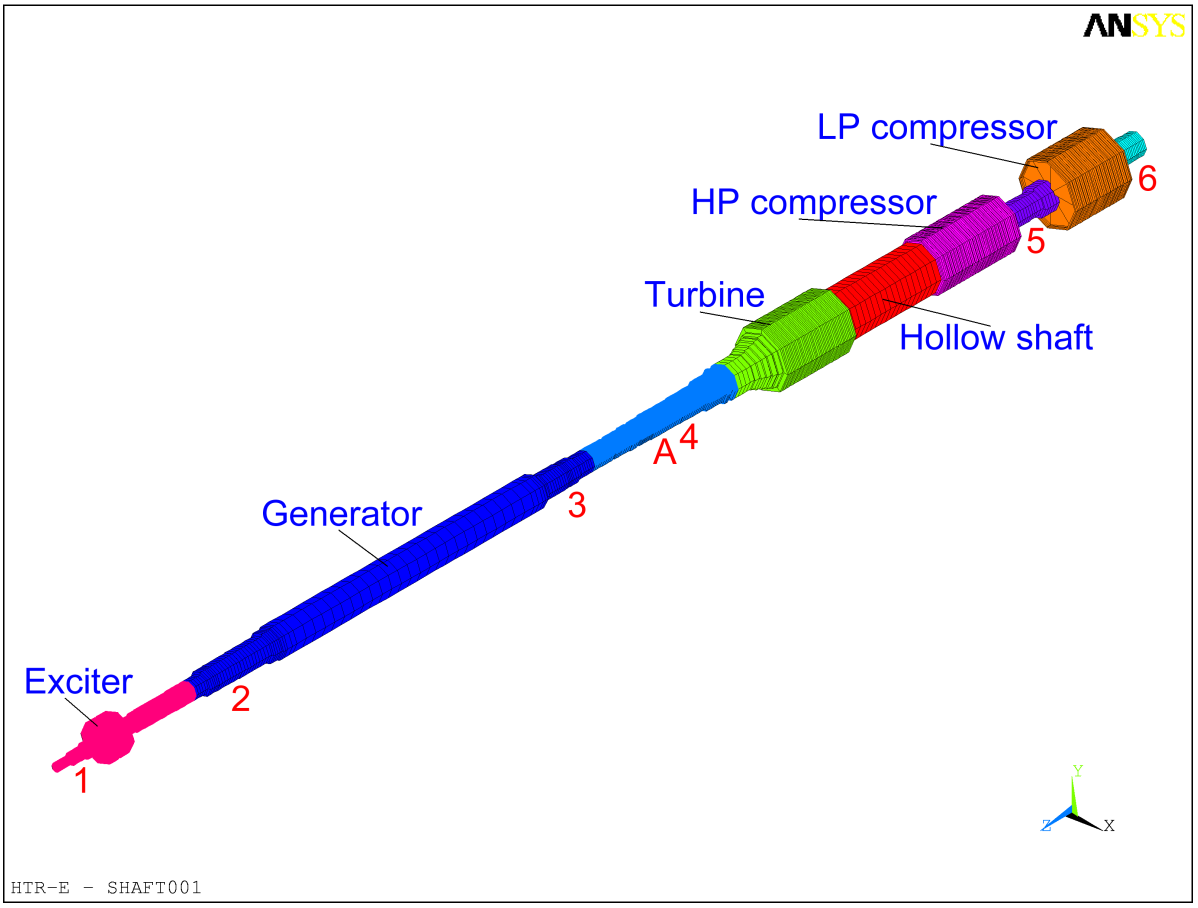


figure 1 Layout of the GT-MHR rotor shaft

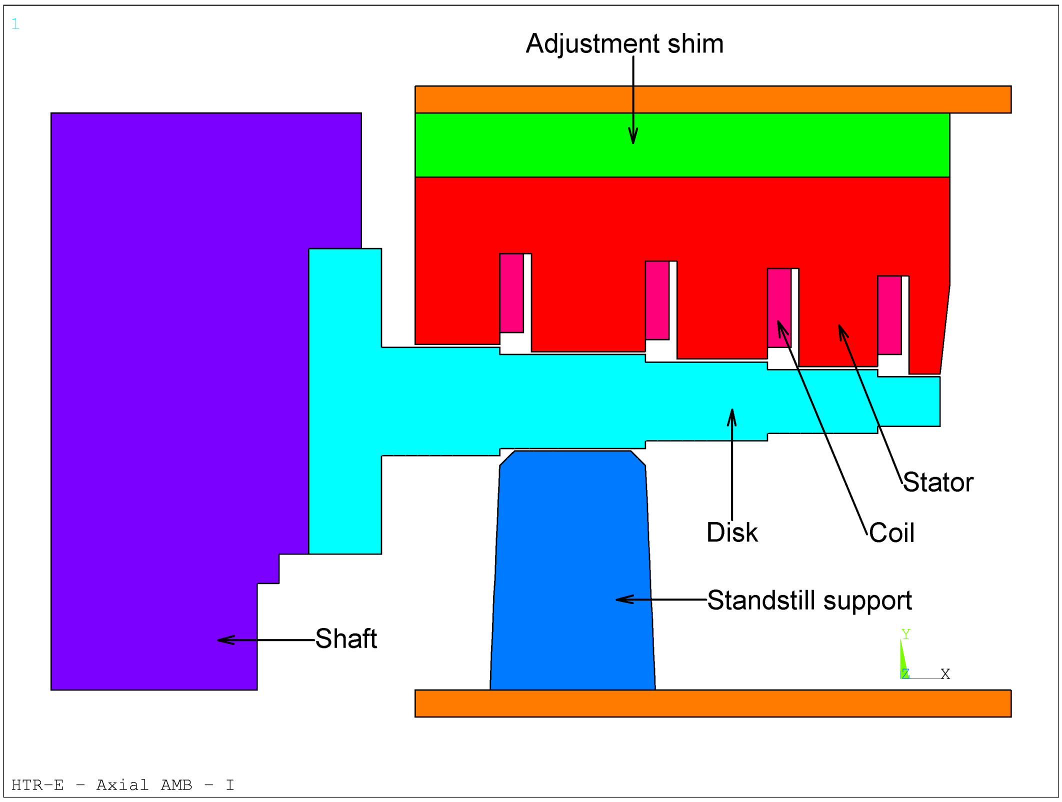


figure 2 Schematic view of the axial Active Magnetic Bearing design as proposed by S2M

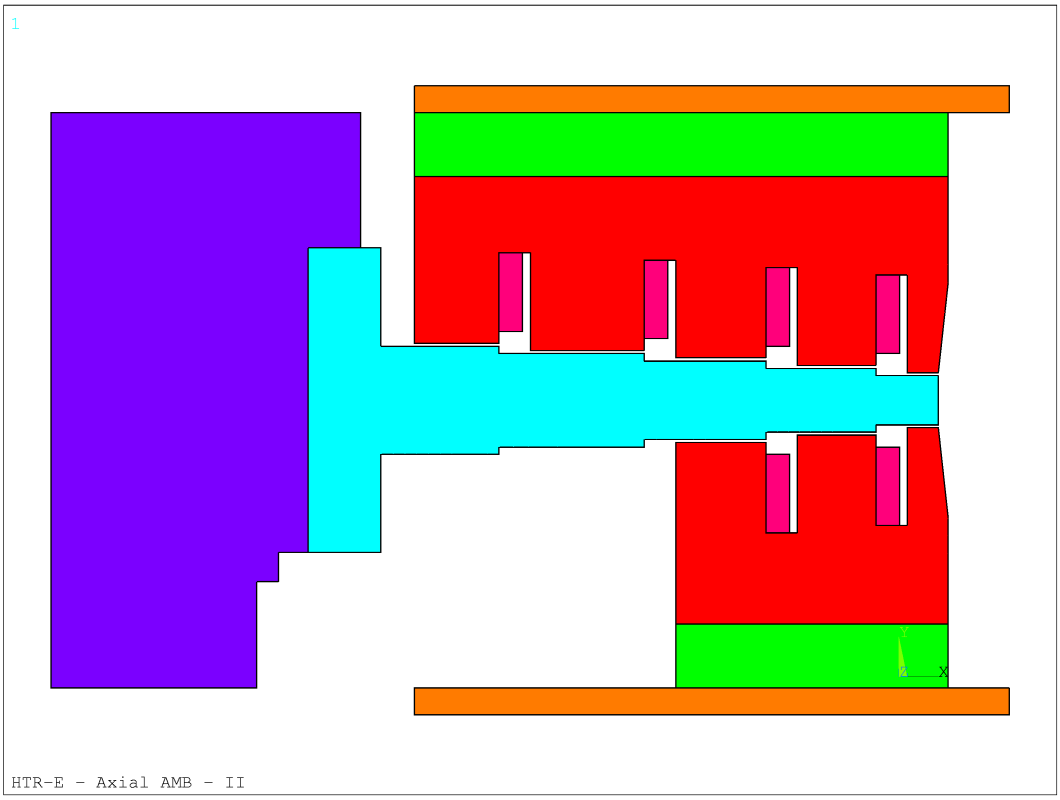


figure 3 Schematic view of the axial Active Magnetic Bearing design providing support for downward and upward rotor loads

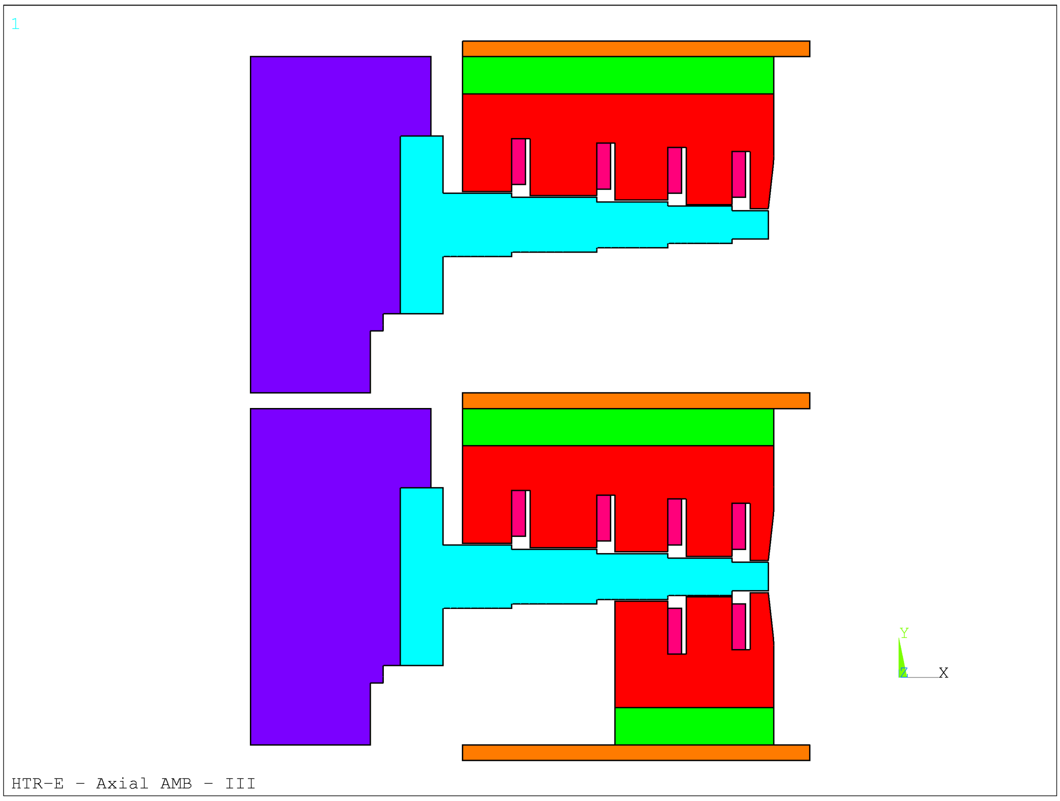


figure 4 Schematic view of the 2-disk axial Active Magnetic Bearing design providing support for downward and upward rotor loads

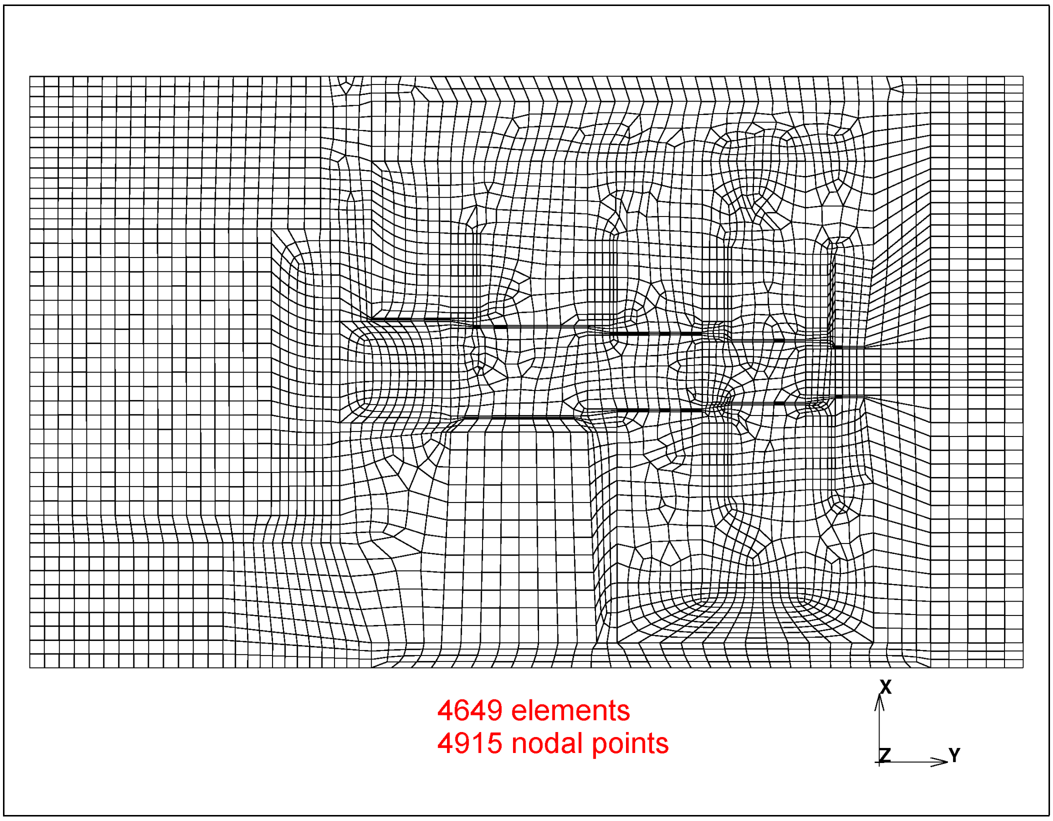


figure 5 The finite element model used for the magnetic and structural calculations

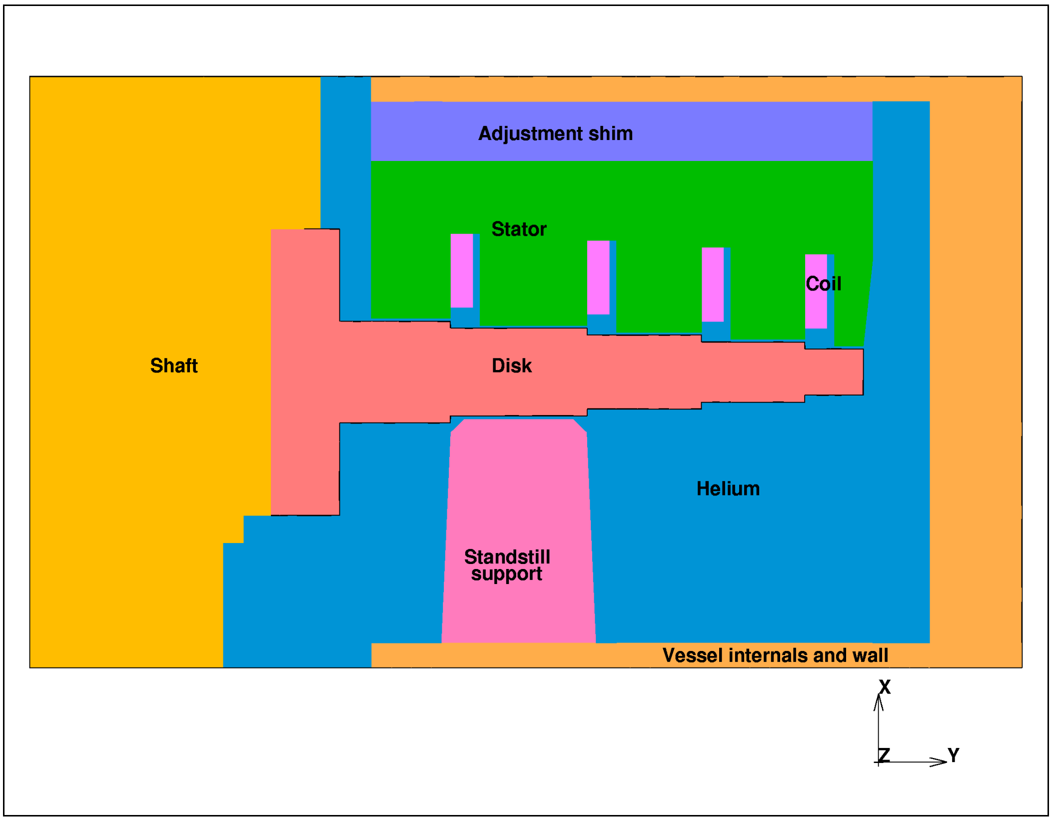


figure 6 Axial Active Magnetic Bearing design I
Geometry and materials

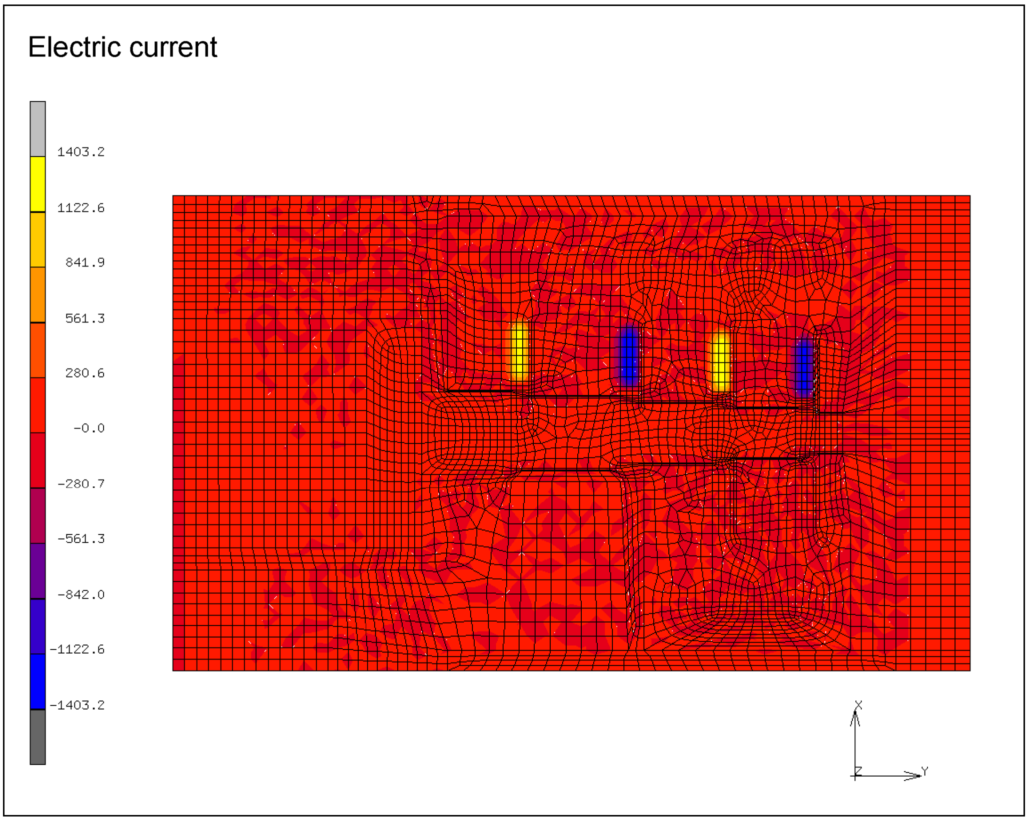


figure 7 Axial Active Magnetic Bearing design I
Electric current distribution [ At ]

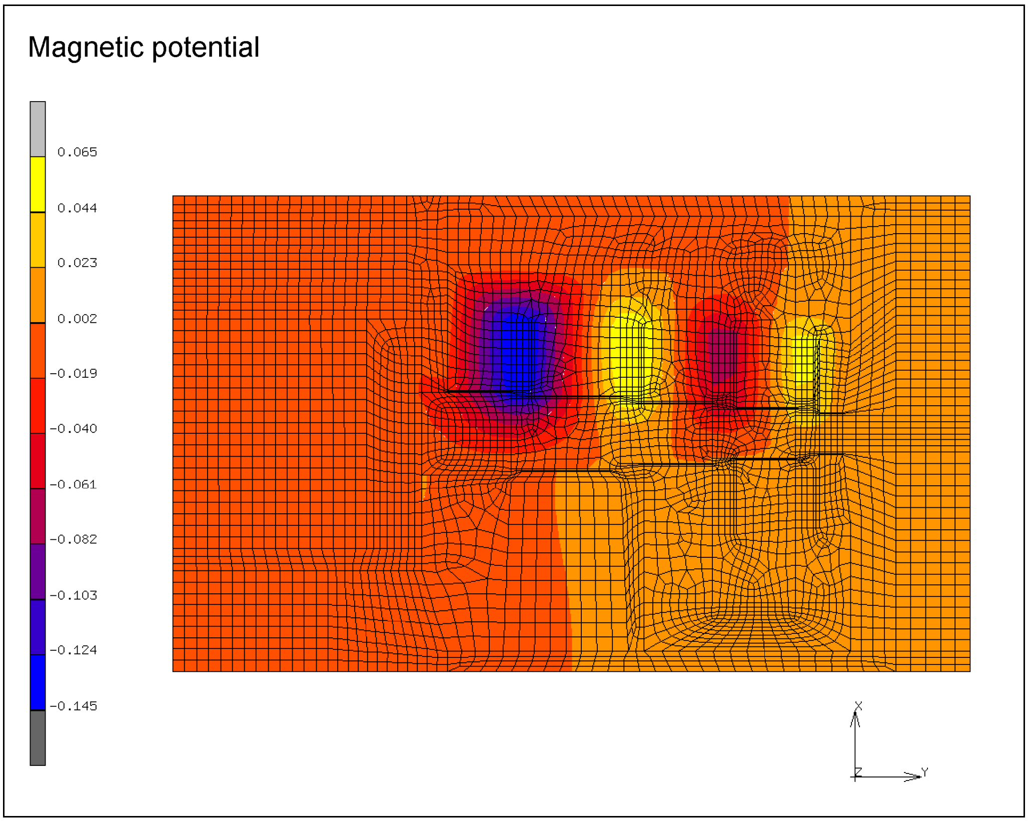


figure 8 Axial Active Magnetic Bearing design I
Magnetic potential distribution [ $A_Z$ ]

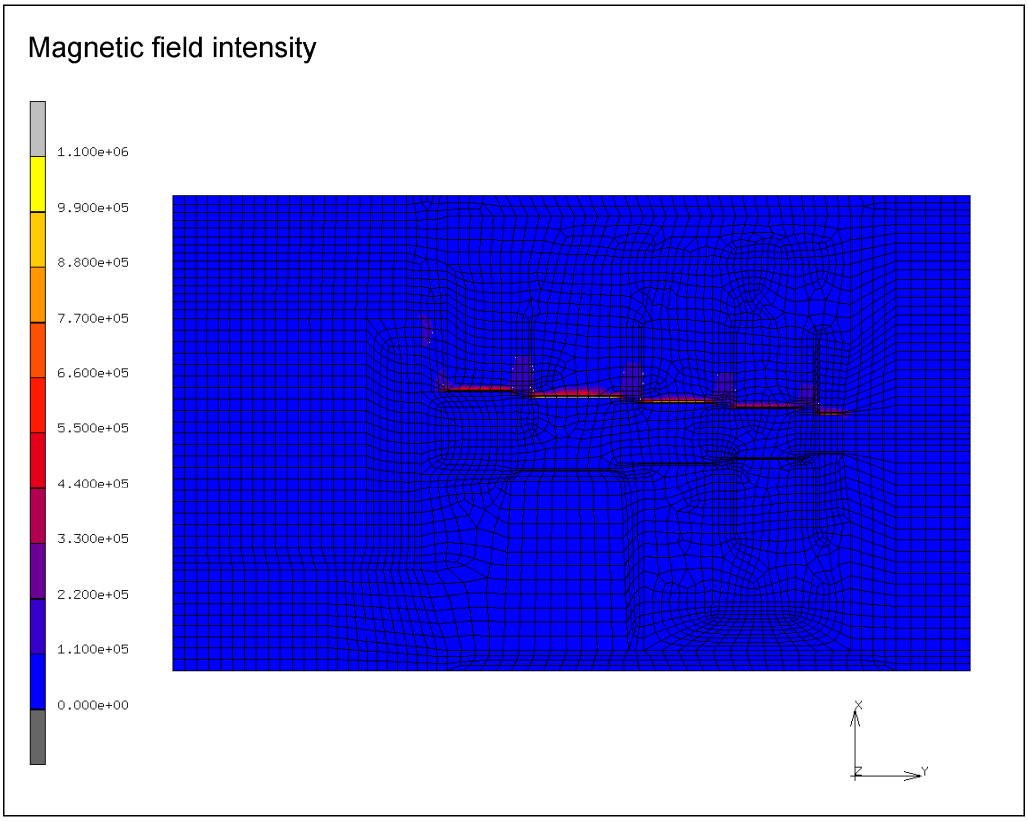


figure 9 Axial Active Magnetic Bearing design I
Distribution of the magnetic field intensity [ H ]

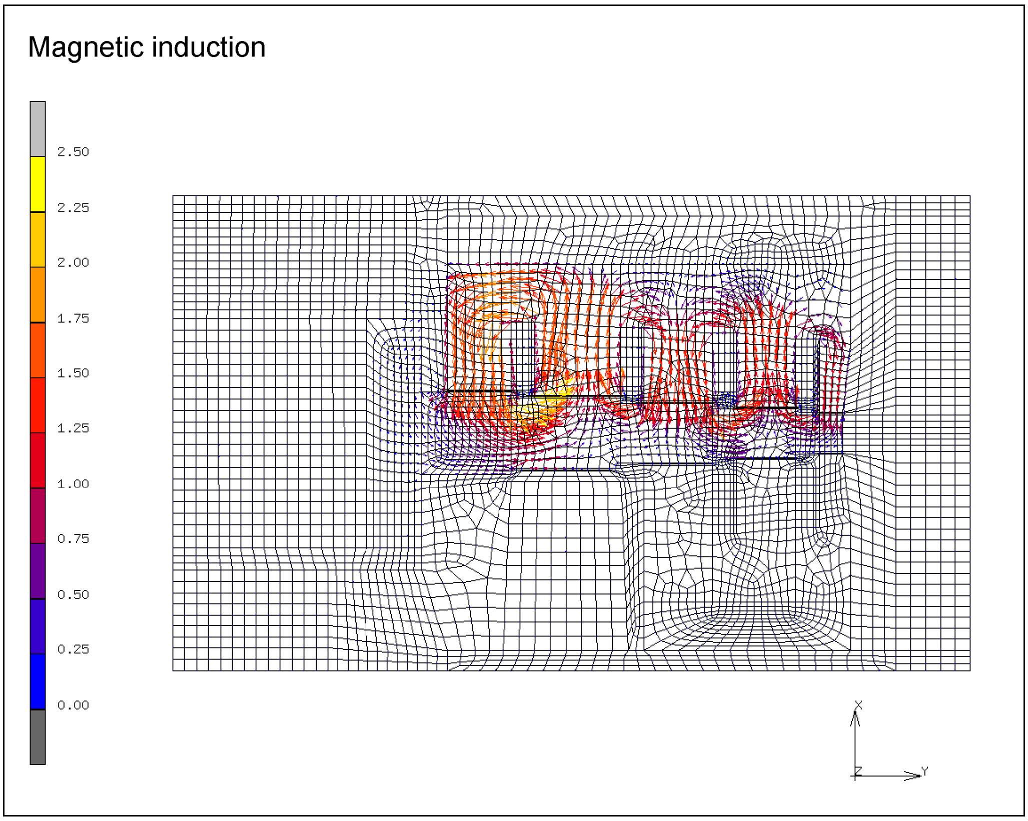


figure 10 Axial Active Magnetic Bearing design I
Magnetic induction [ T ]

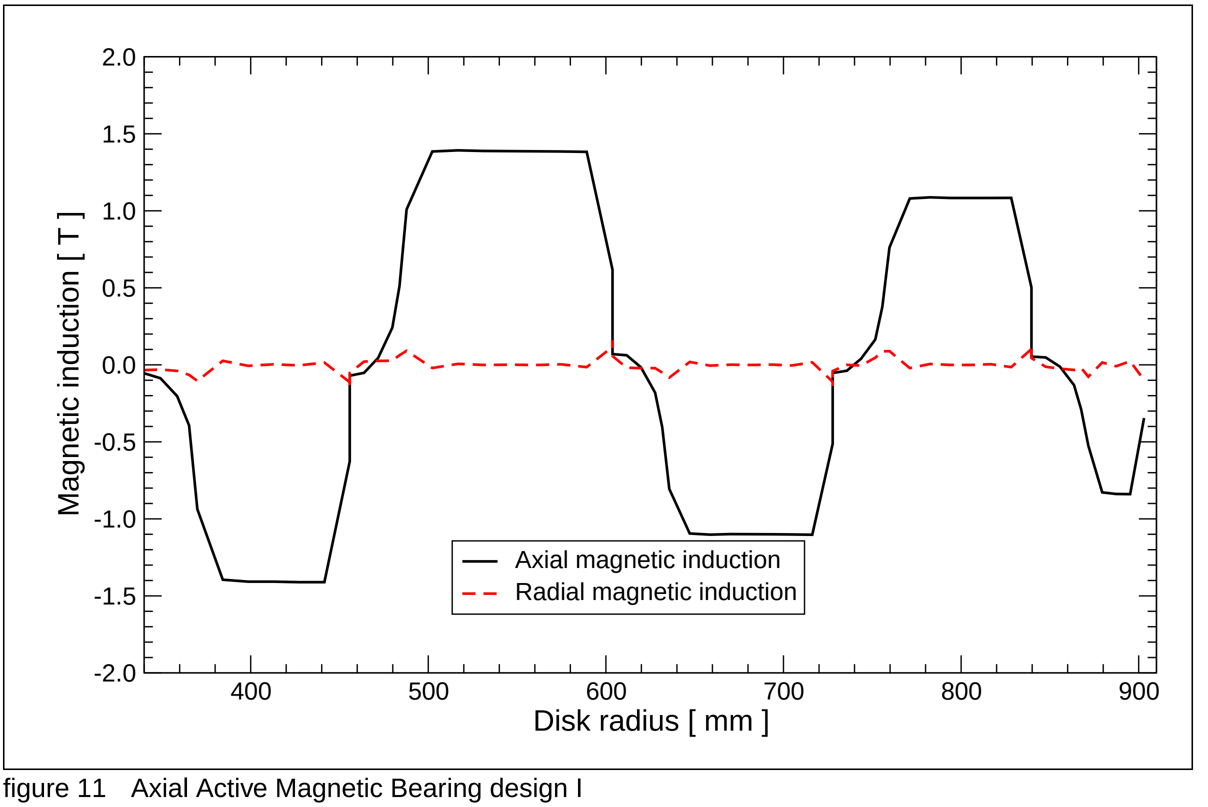


figure 11 Axial Active Magnetic Bearing design I
The magnetic induction in the gap between the stator and the disk

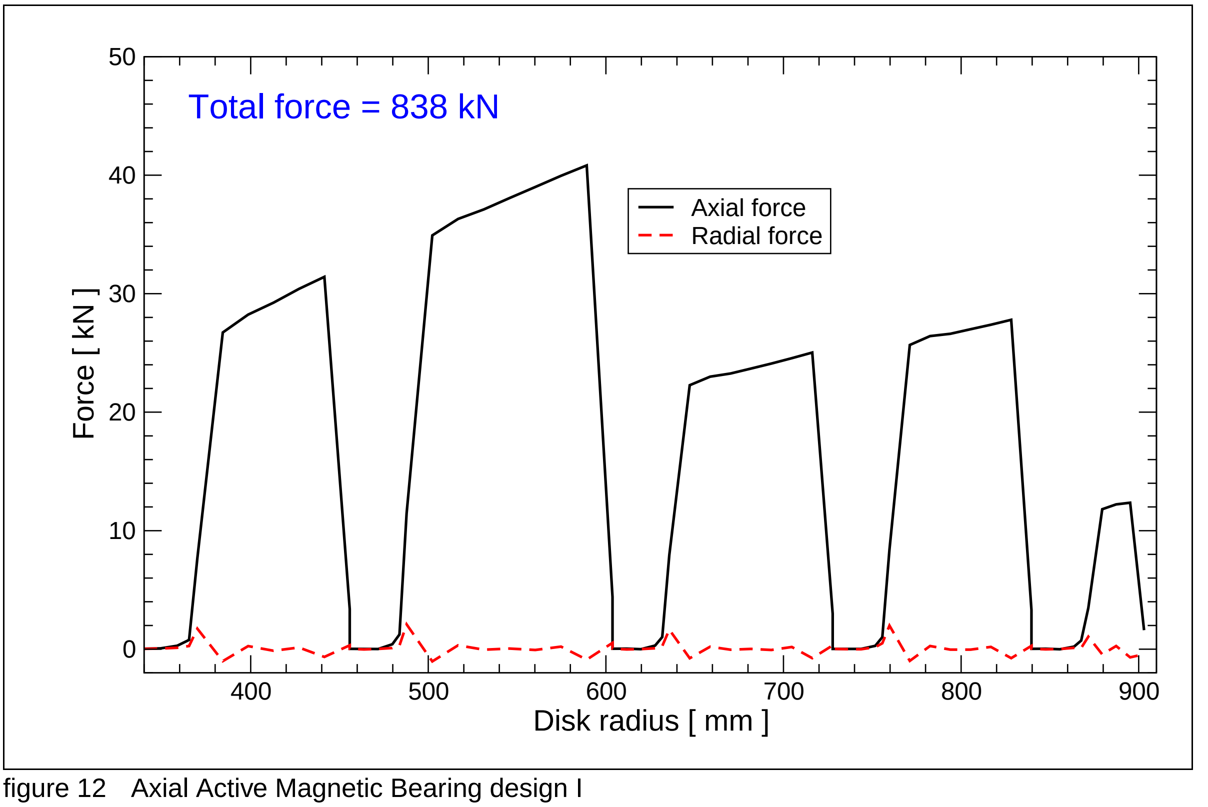


figure 12 Axial Active Magnetic Bearing design I
The magnetic forces on the disk

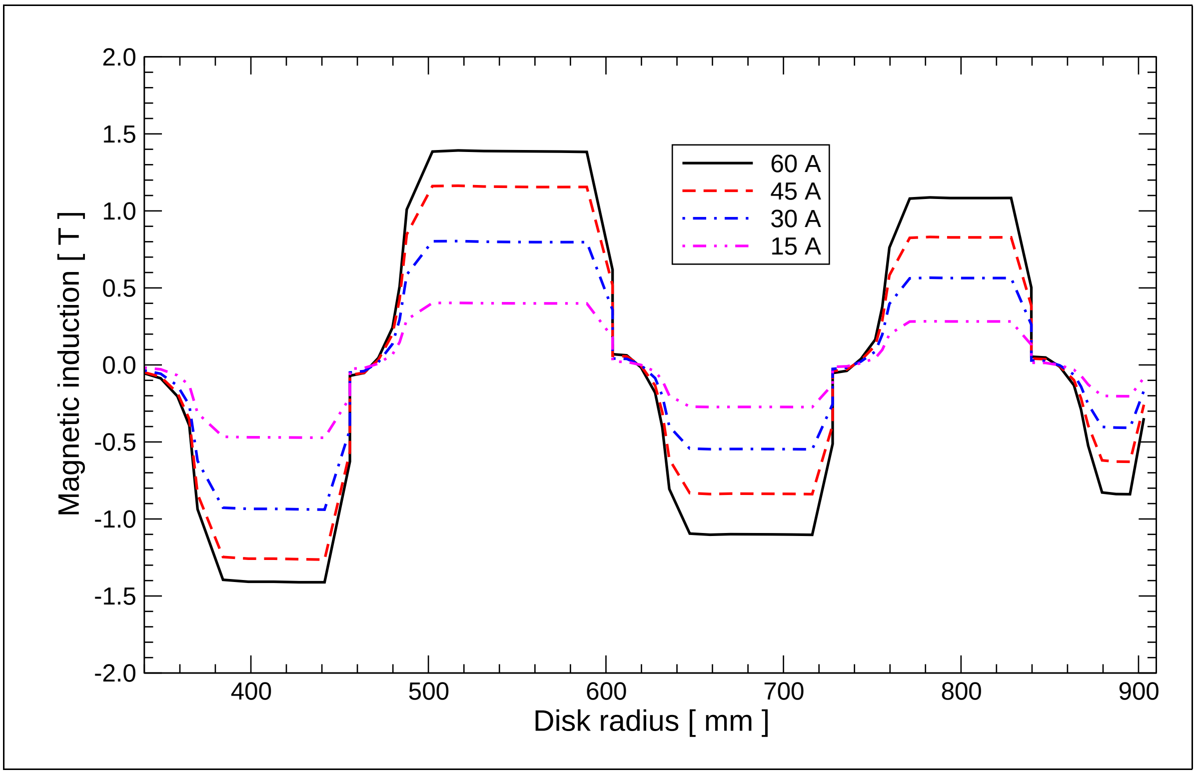


figure 13 Axial Active Magnetic Bearing design I
The magnetic induction in the gap between the stator and the disk as a function of the electric current

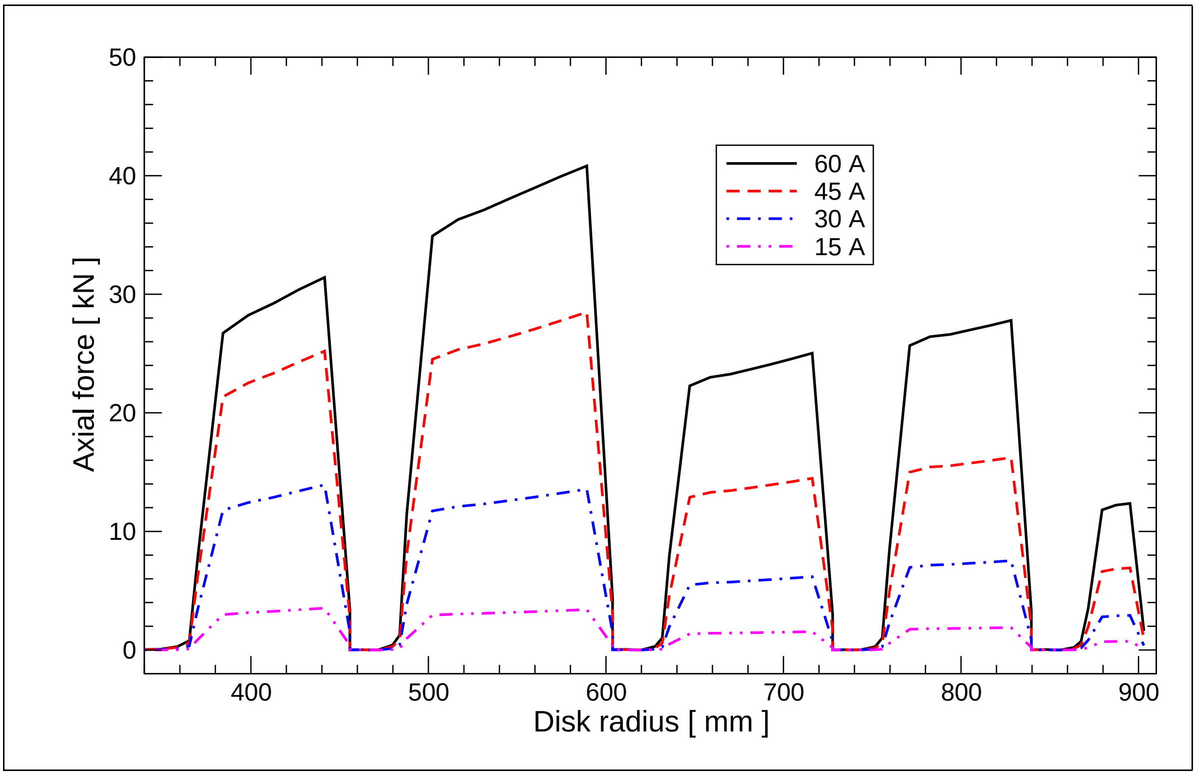


figure 14 Axial Active Magnetic Bearing design I
The magnetic forces on the disk as a function of the electric current

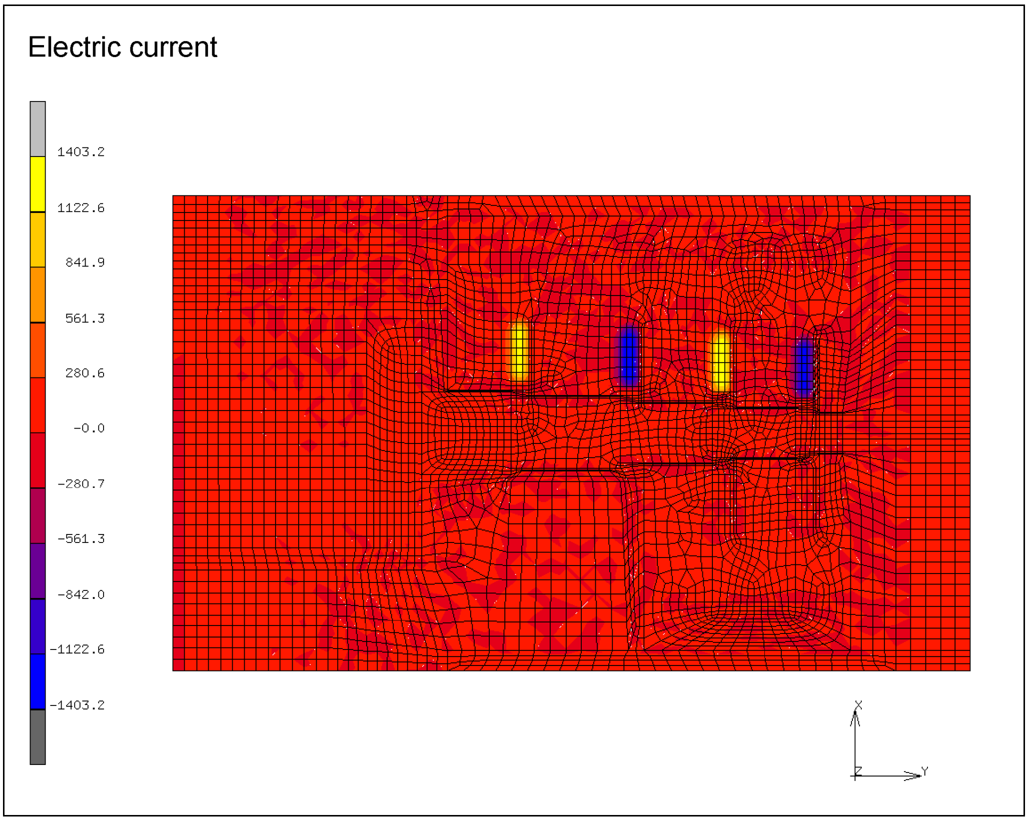


figure 15 Axial Active Magnetic Bearing design II
Electric current distribution (lift mode) [ At ]

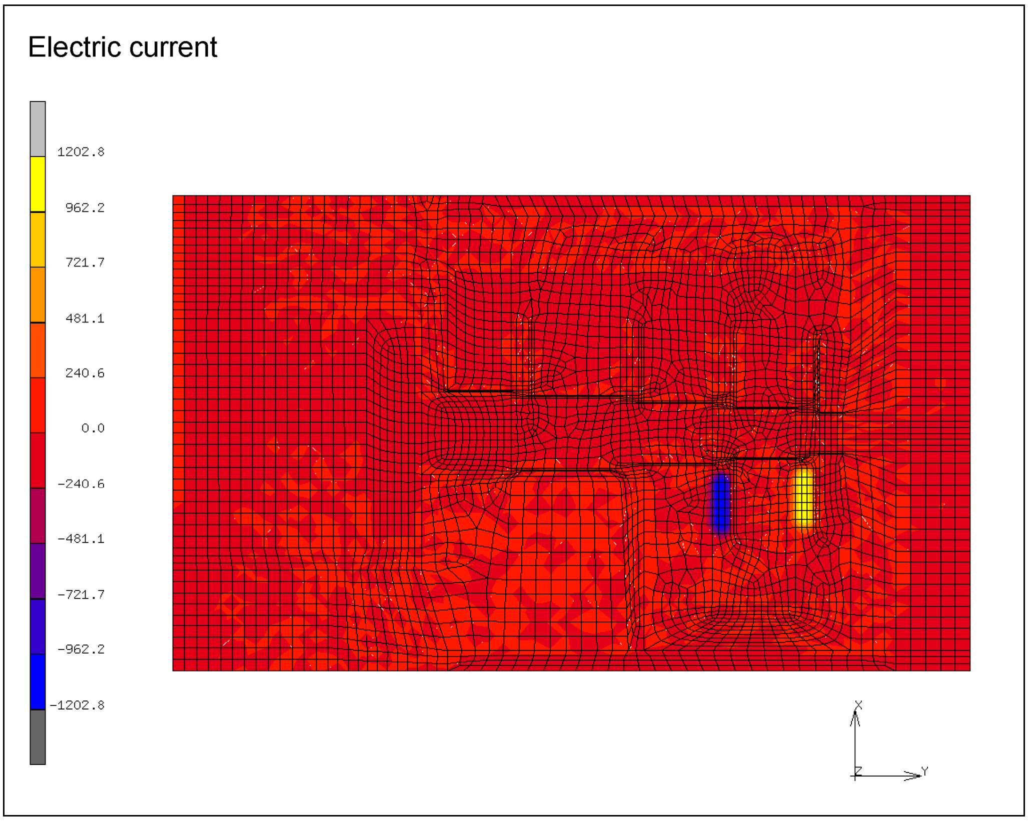


figure 16 Axial Active Magnetic Bearing design II
Electric current distribution (pull mode) [ At ]

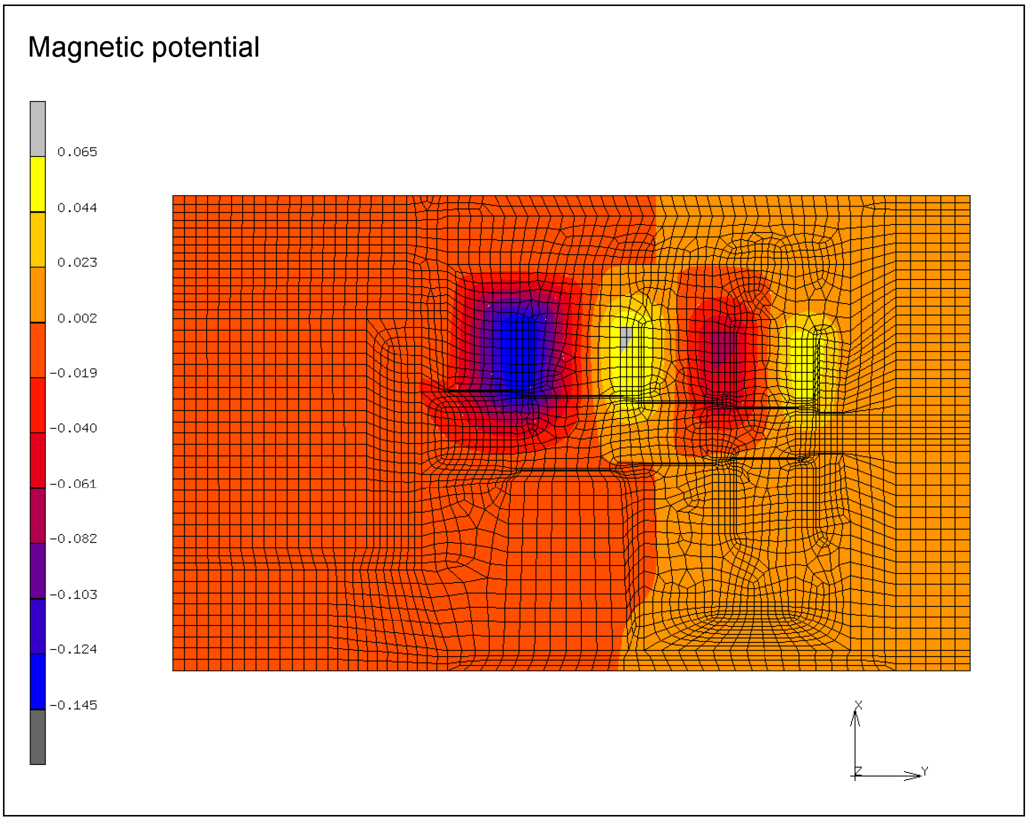


figure 17 Axial Active Magnetic Bearing design II
Magnetic potential distribution (lift mode) [ $A_Z$ ]

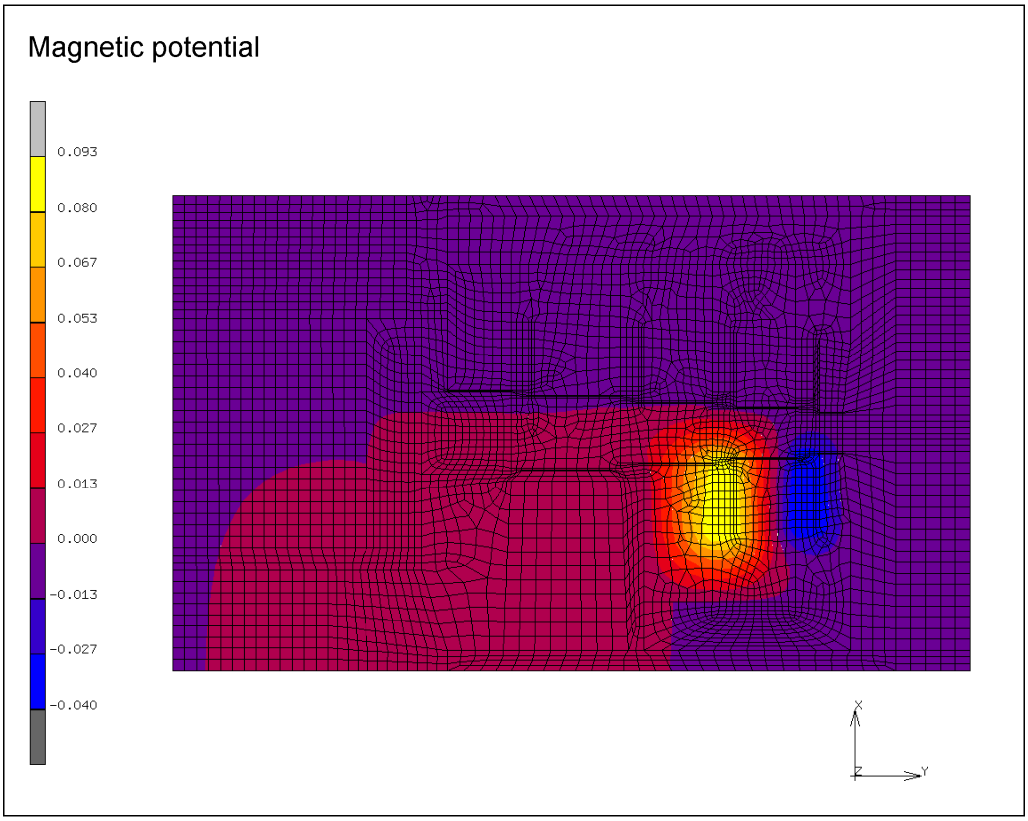


figure 18 Axial Active Magnetic Bearing design II
Magnetic potential distribution (pull mode) [ $A_Z$ ]

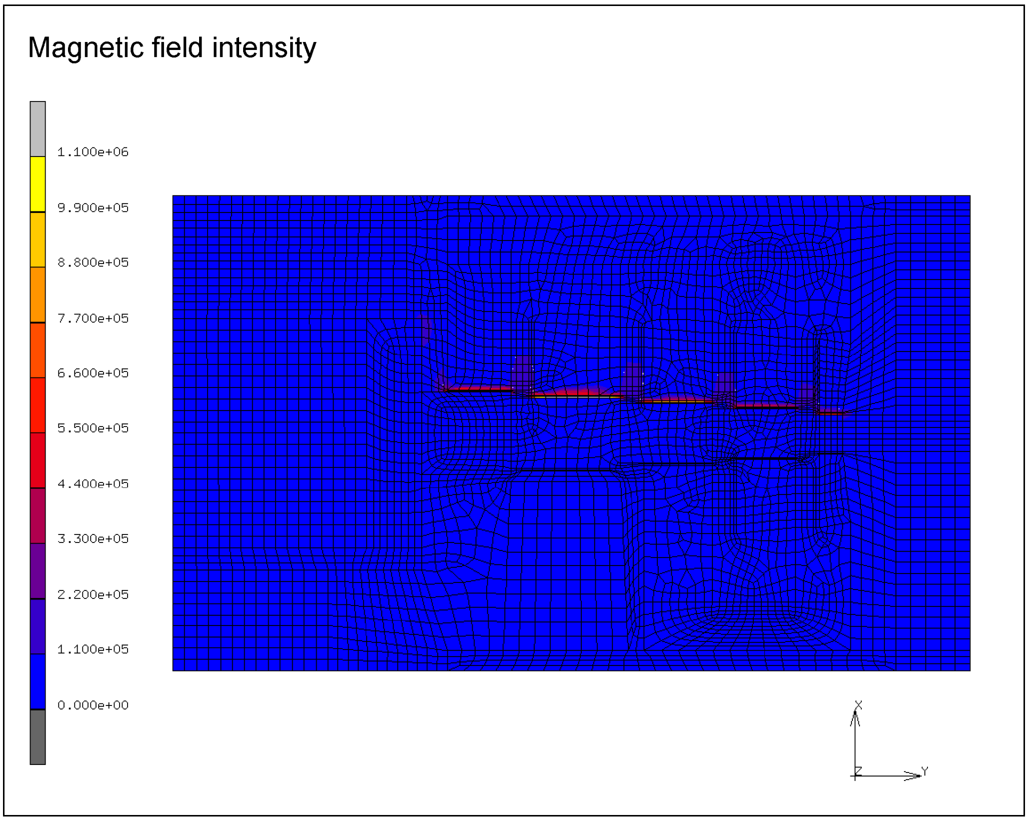


figure 19 Axial Active Magnetic Bearing design II
Distribution of the magnetic field intensity (lift mode) [ H ]

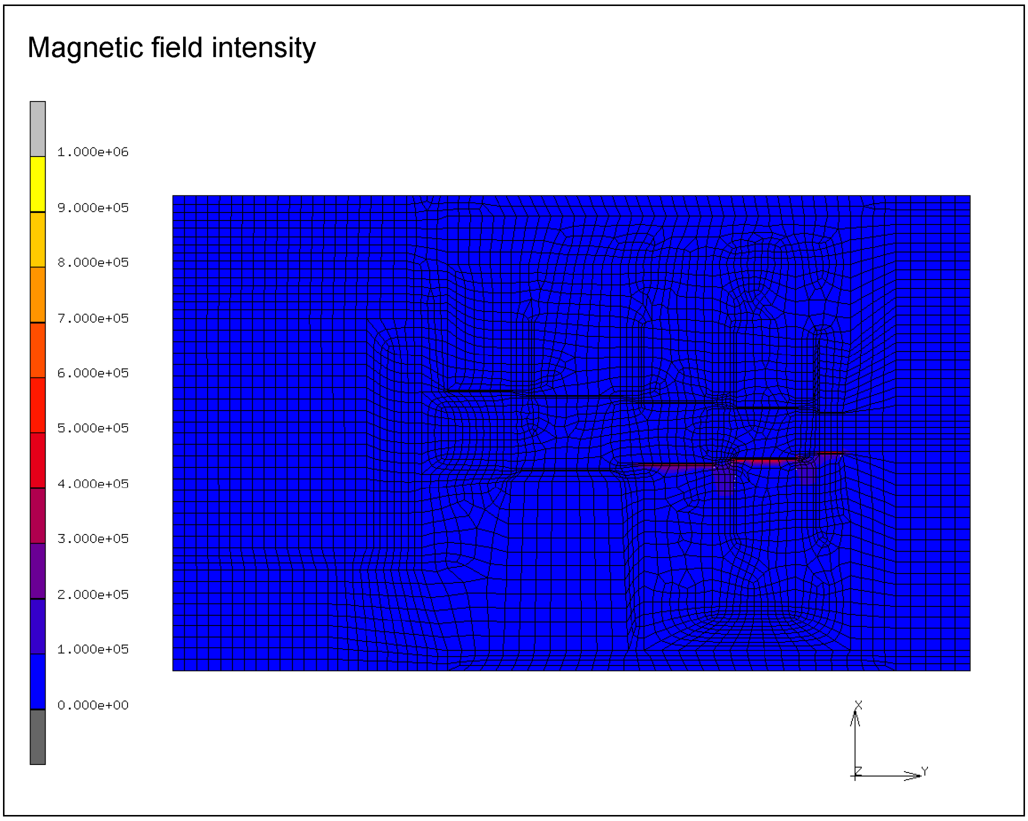


figure 20 Axial Active Magnetic Bearing design II
Distribution of the magnetic field intensity (pull mode) [ H ]

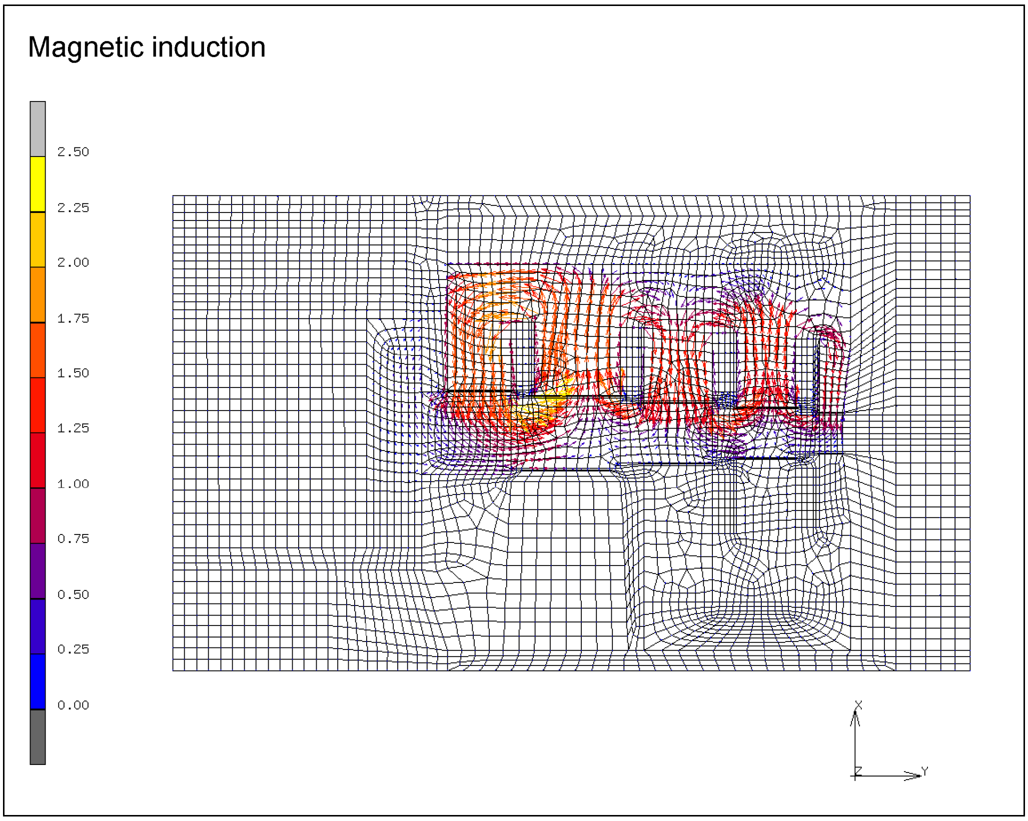


figure 21 Axial Active Magnetic Bearing design II
Magnetic induction (lift mode) [ T ]

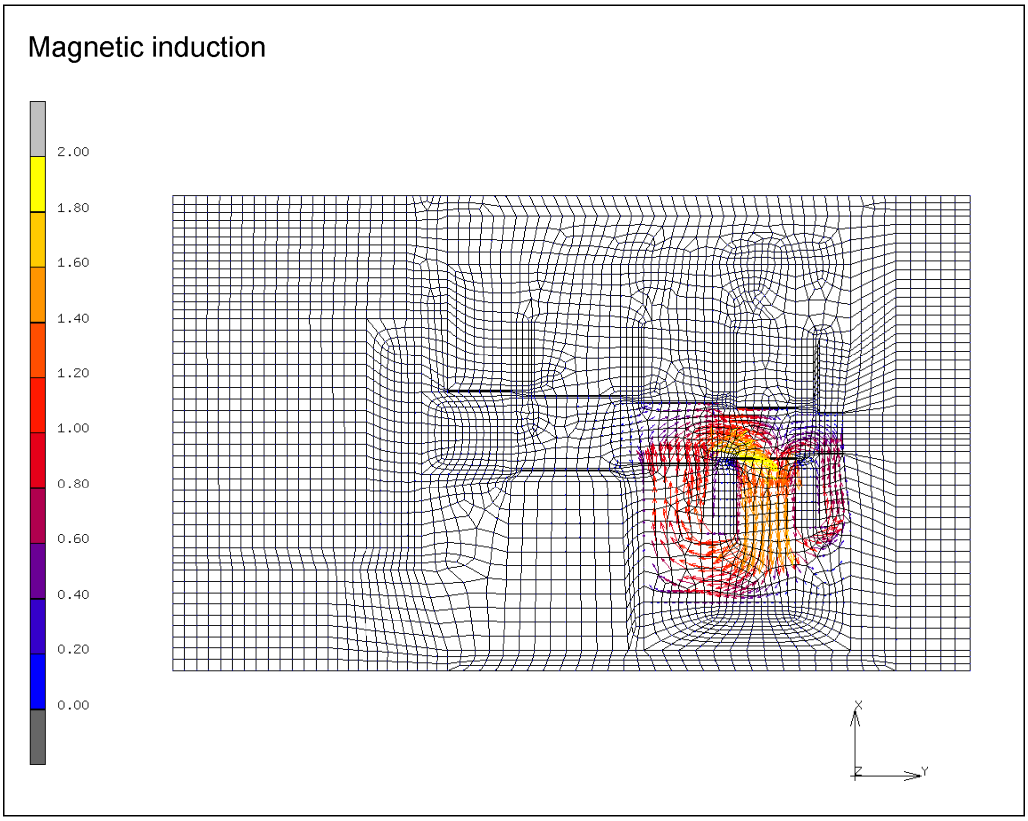


figure 22 Axial Active Magnetic Bearing design II
Magnetic induction (pull mode) [ T ]

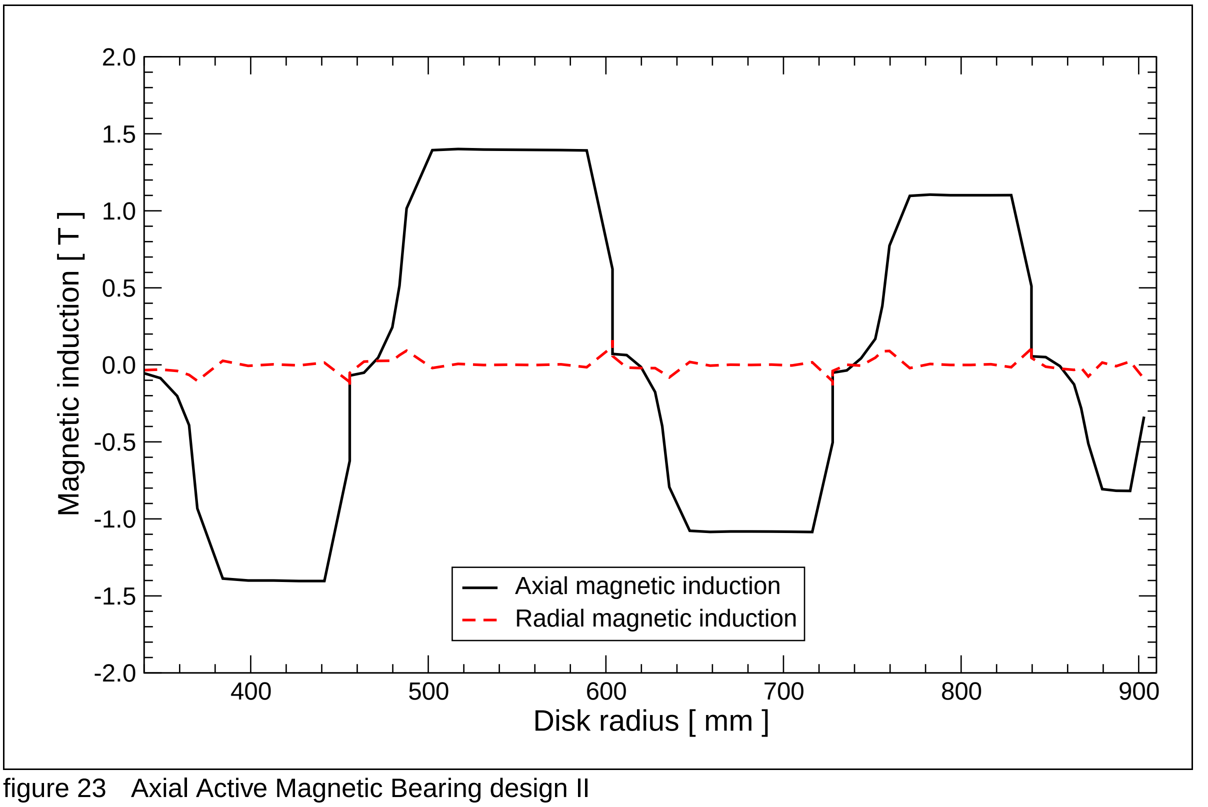


figure 23 Axial Active Magnetic Bearing design II
The magnetic induction in the gap between the stator and the disk (lift mode)

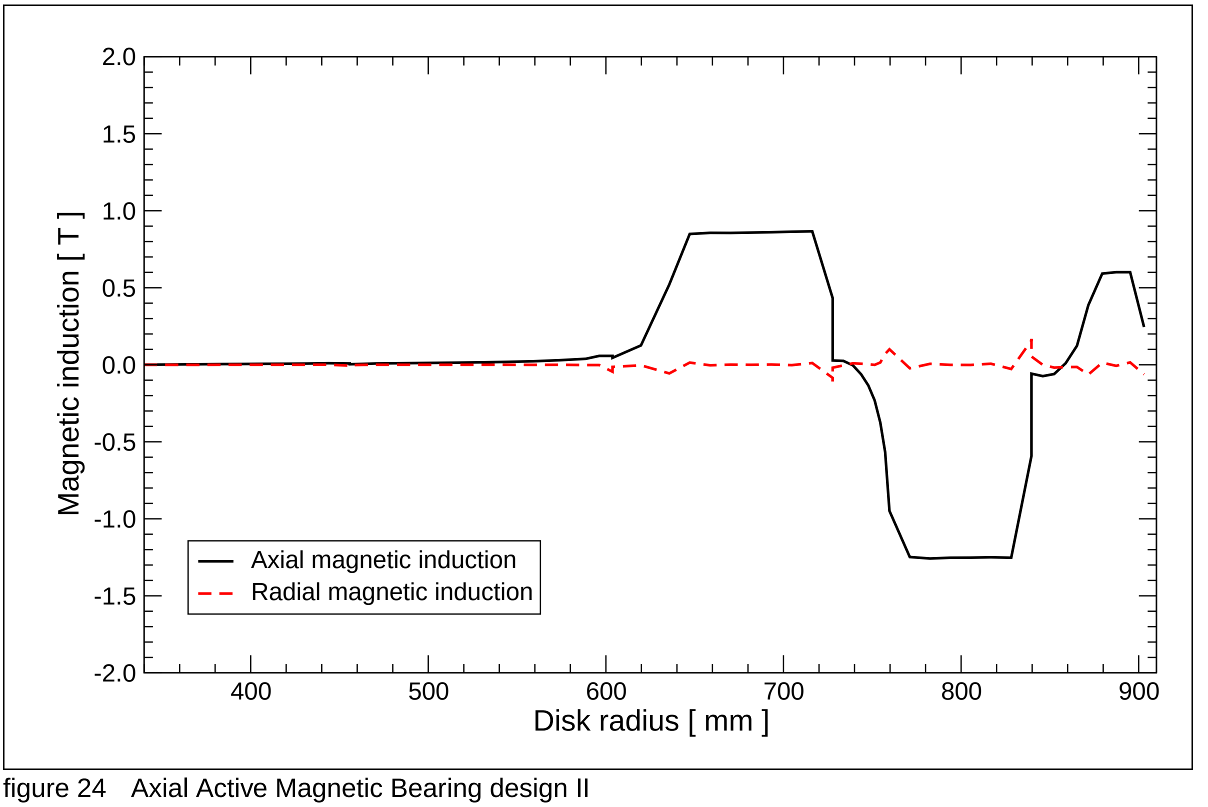


figure 24 Axial Active Magnetic Bearing design II
The magnetic induction in the gap between the stator and the disk (pull mode)

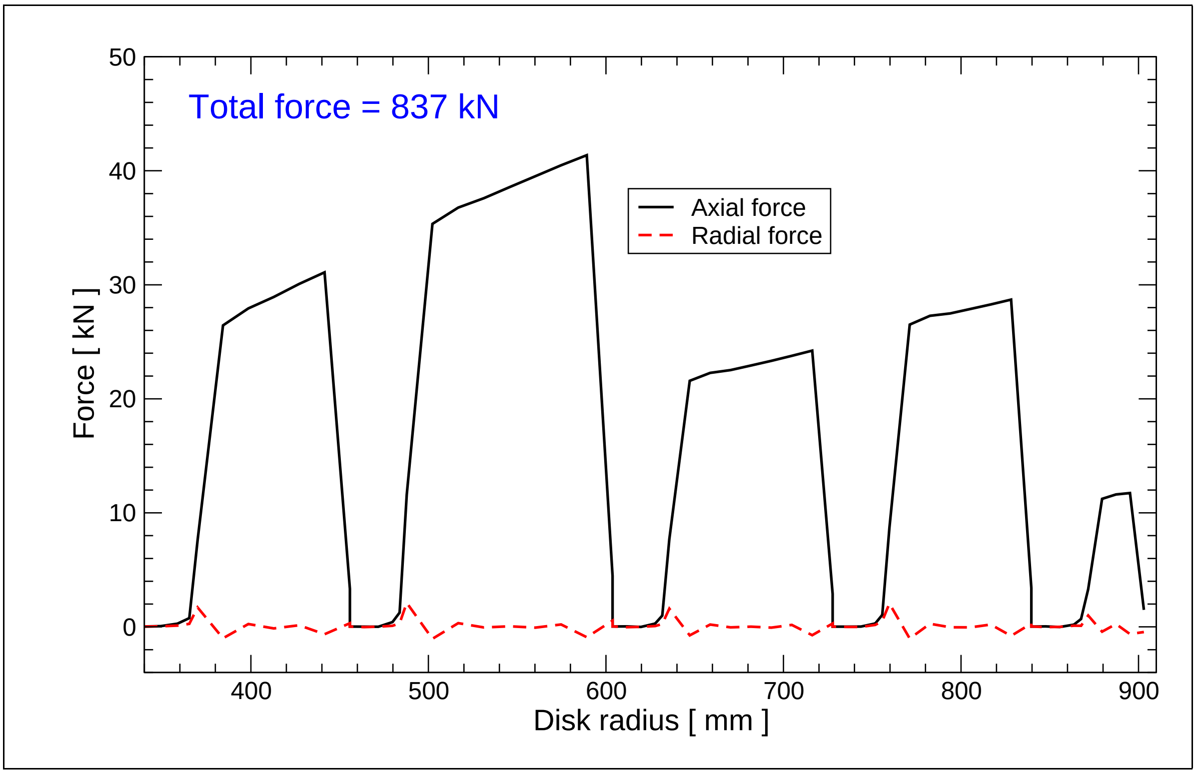


figure 25 Axial Active Magnetic Bearing design II
The magnetic forces on the disk (lift mode)

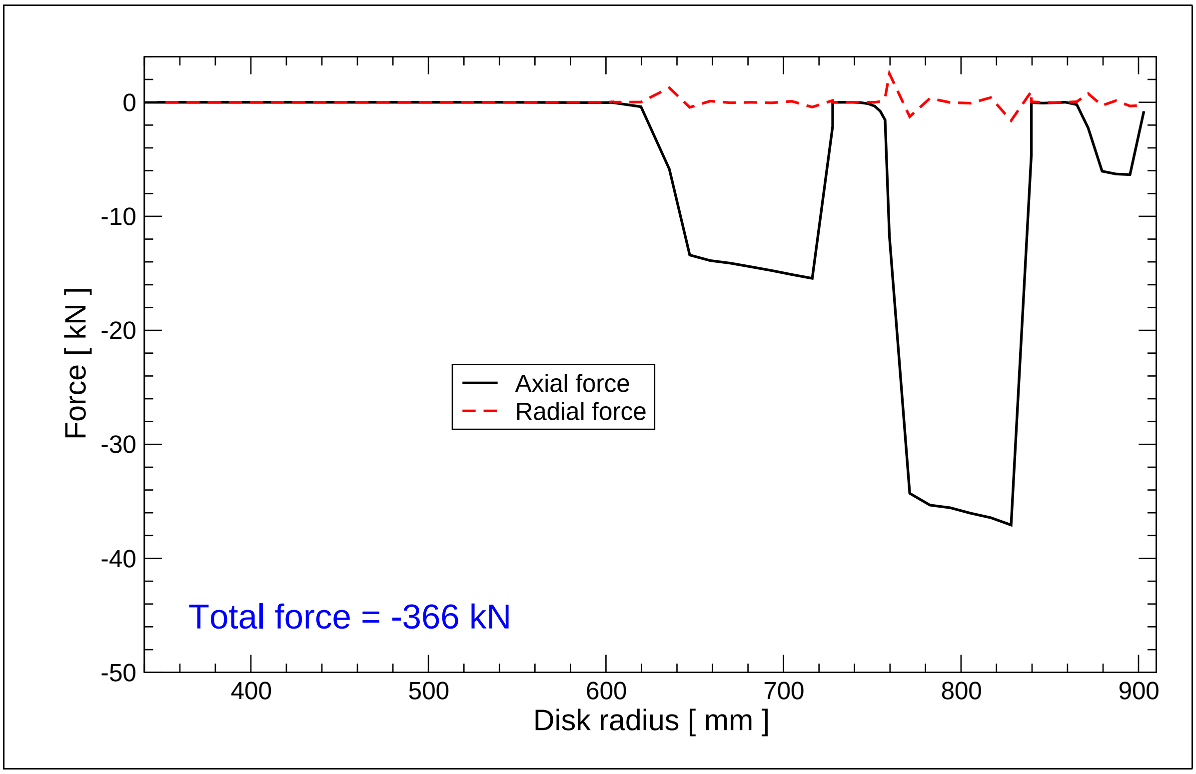


figure 26 Axial Active Magnetic Bearing design II
The magnetic forces on the disk (pull mode)

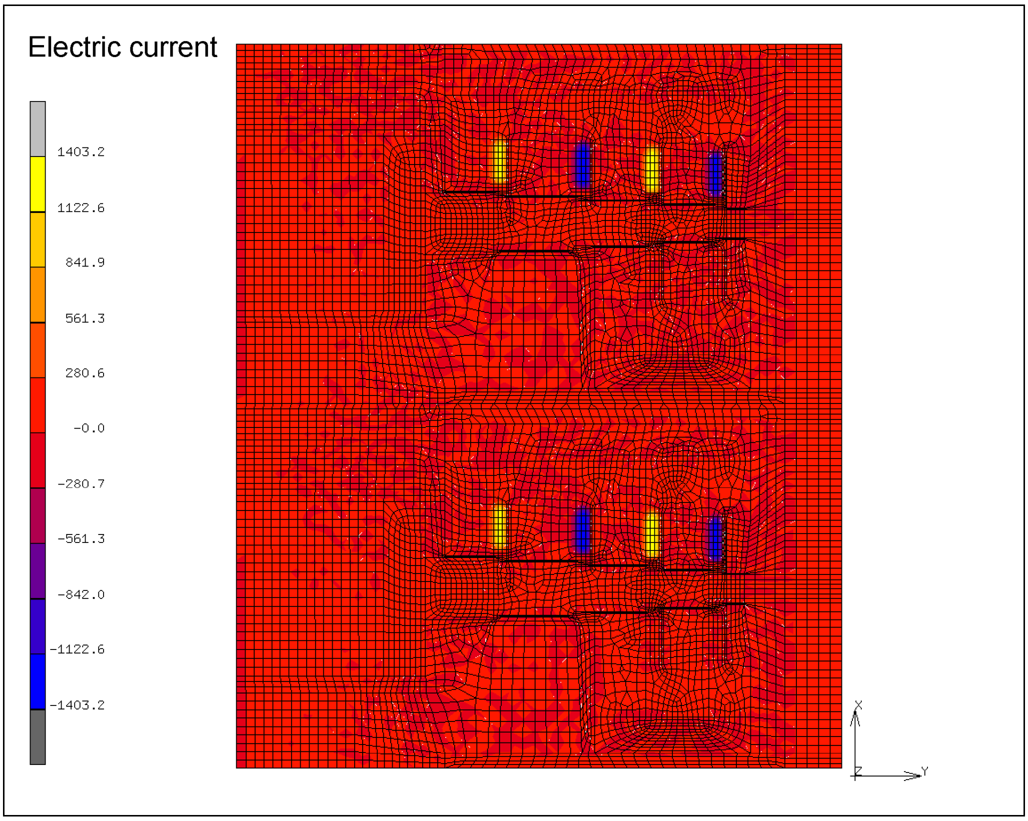


figure 27 Axial Active Magnetic Bearing design III
Electric current distribution (lift mode) [ At ]

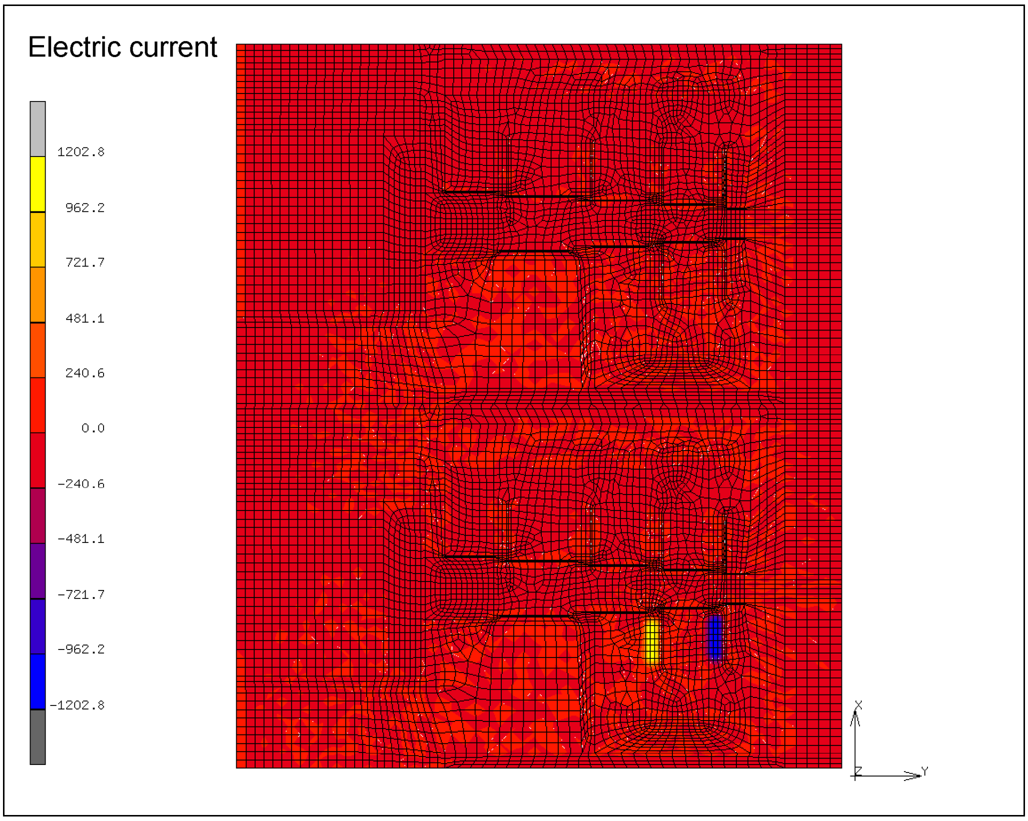


figure 28 Axial Active Magnetic Bearing design III
Electric current distribution (pull mode) [ At ]

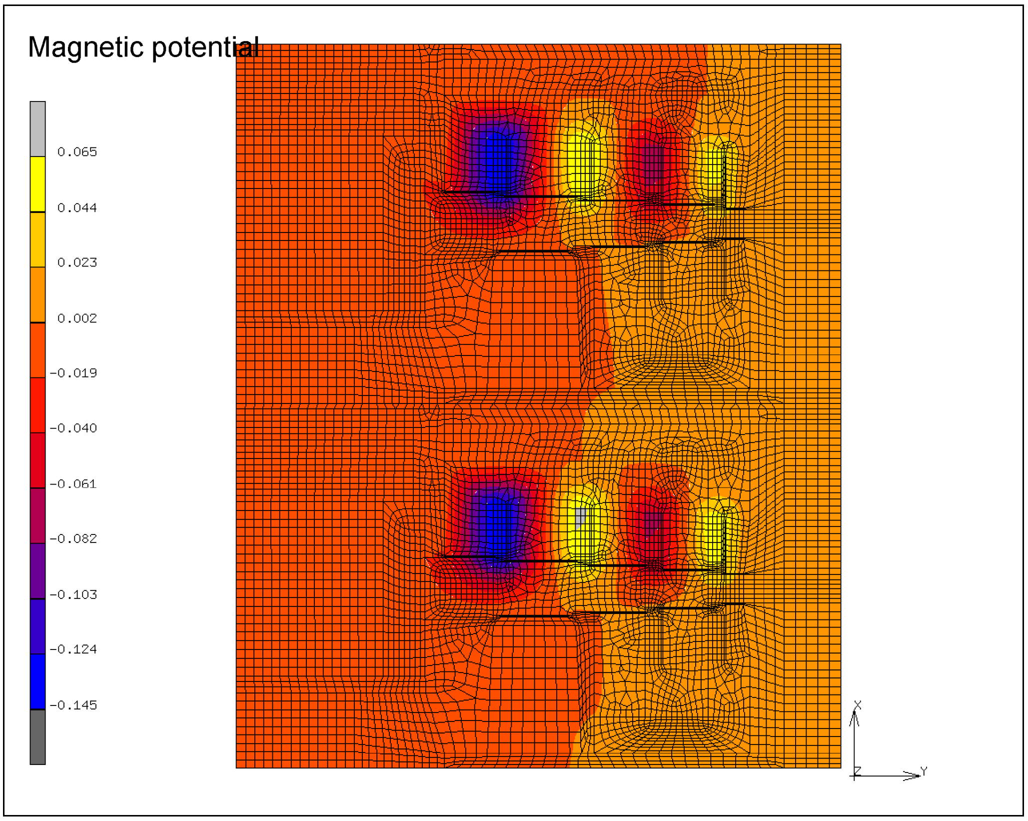


figure 29 Axial Active Magnetic Bearing design III
Magnetic potential distribution (lift mode) [ $A_Z$ ]

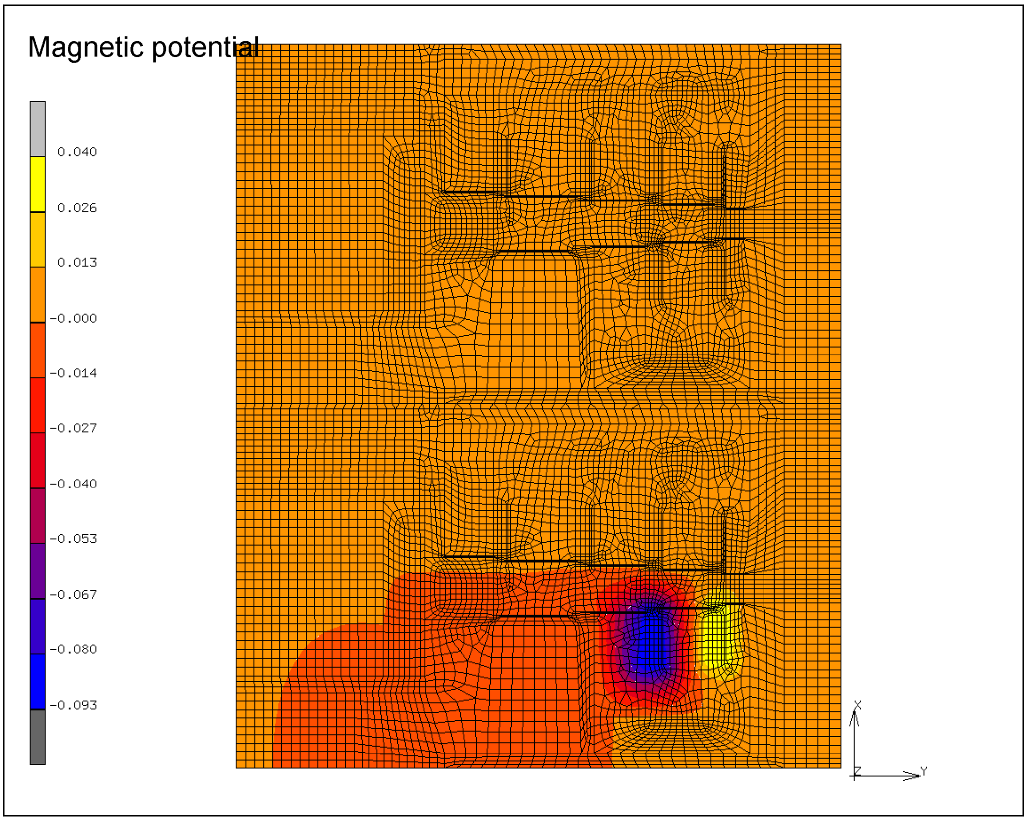


figure 30 Axial Active Magnetic Bearing design III
Magnetic potential distribution (pull mode) [ $A_Z$ ]

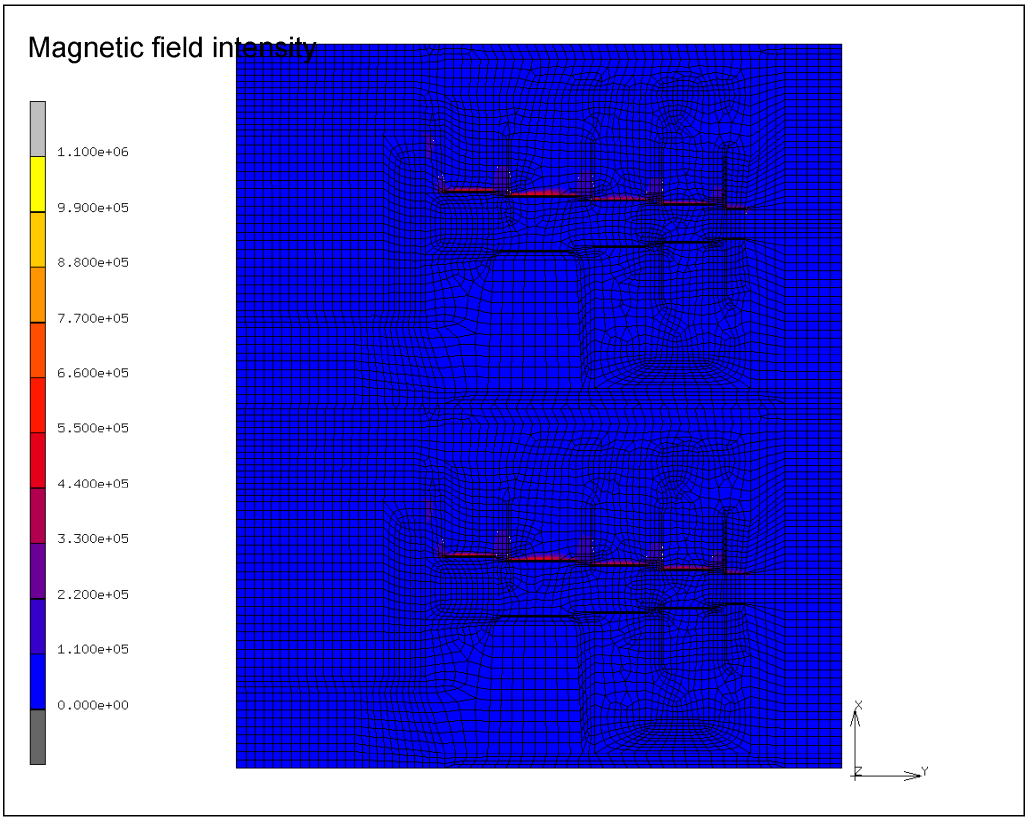


figure 31 Axial Active Magnetic Bearing design III
Distribution of the magnetic field intensity (lift mode) [ H ]

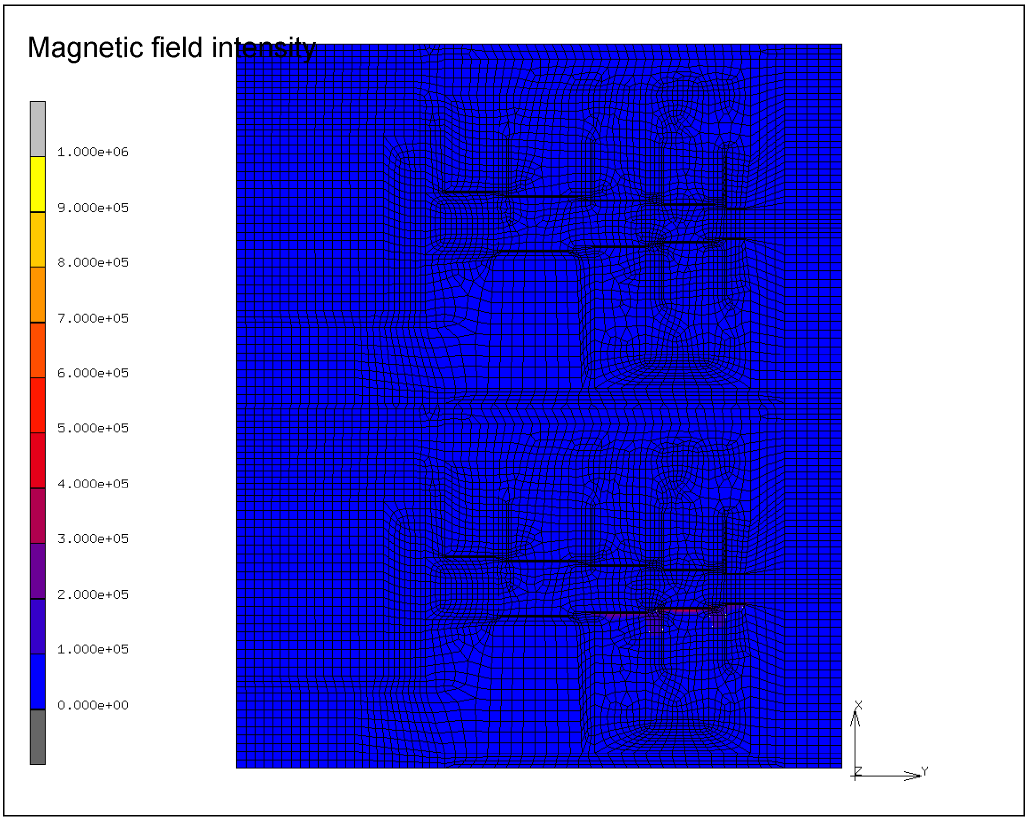


figure 32 Axial Active Magnetic Bearing design III
Distribution of the magnetic field intensity (pull mode) [ H ]

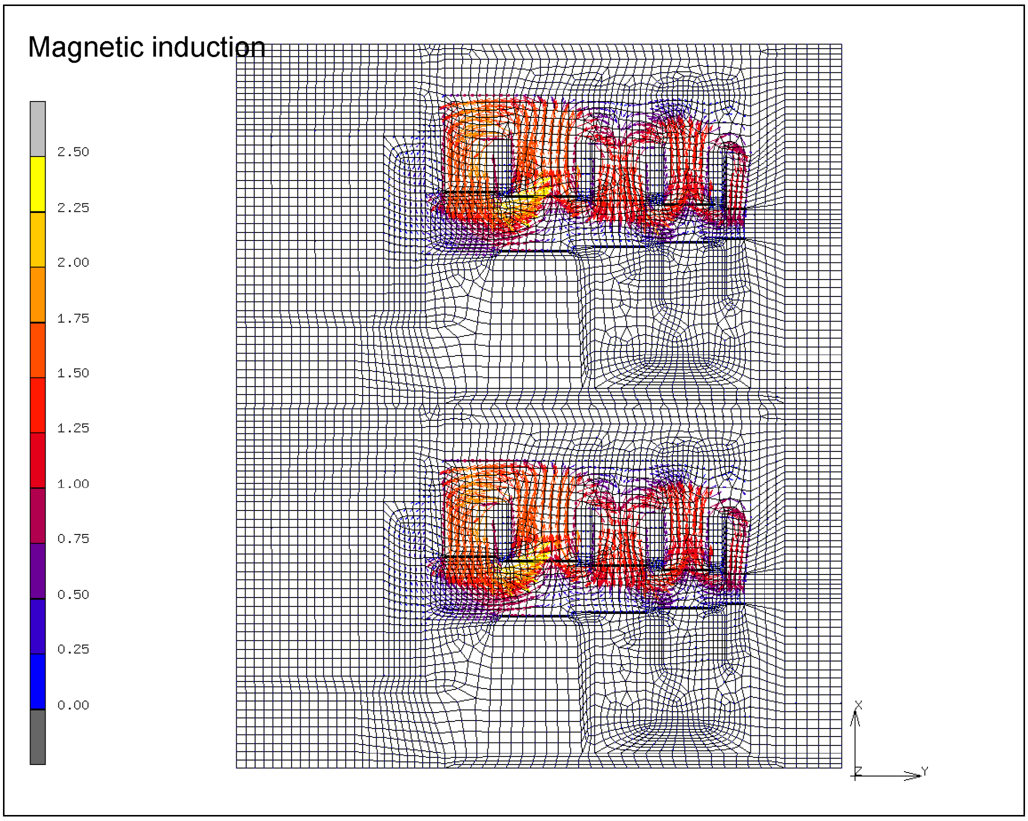


figure 33 Axial Active Magnetic Bearing design III
Magnetic induction (lift mode) [ T ]

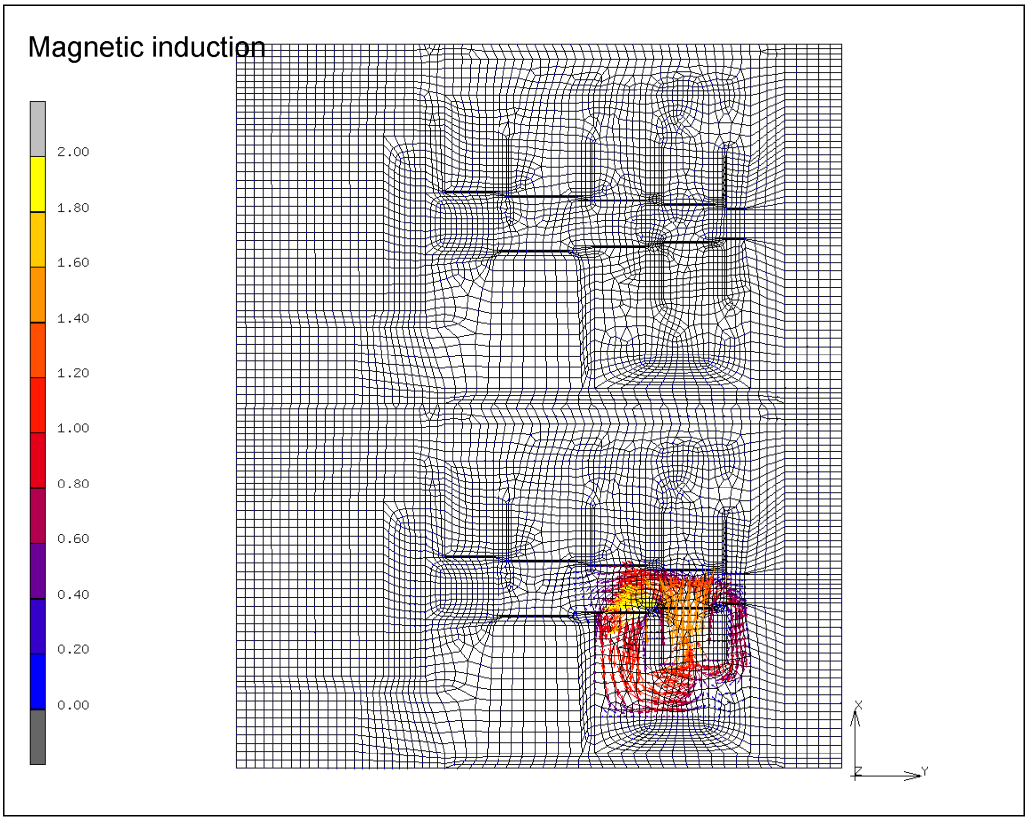


figure 34 Axial Active Magnetic Bearing design III
Magnetic induction (pull mode) [ T ]

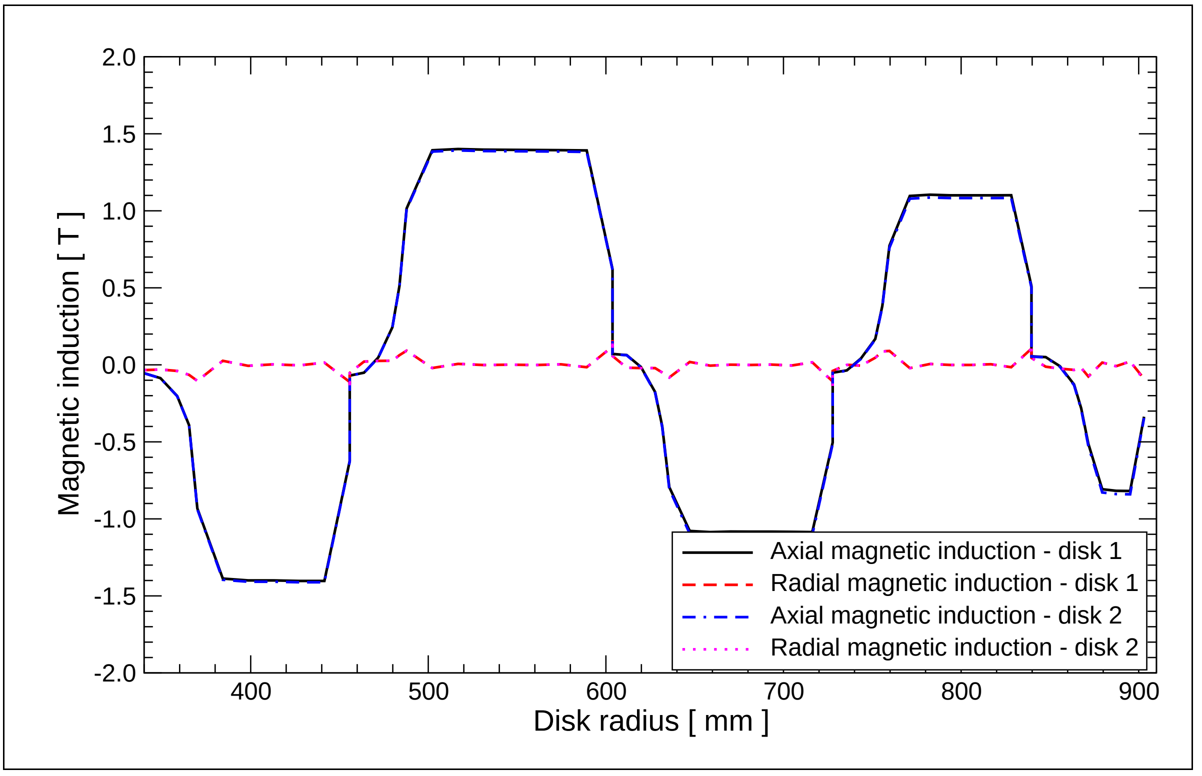


figure 35 Axial Active Magnetic Bearing design III
The magnetic induction in the gap between the stator and the disk (lift mode)

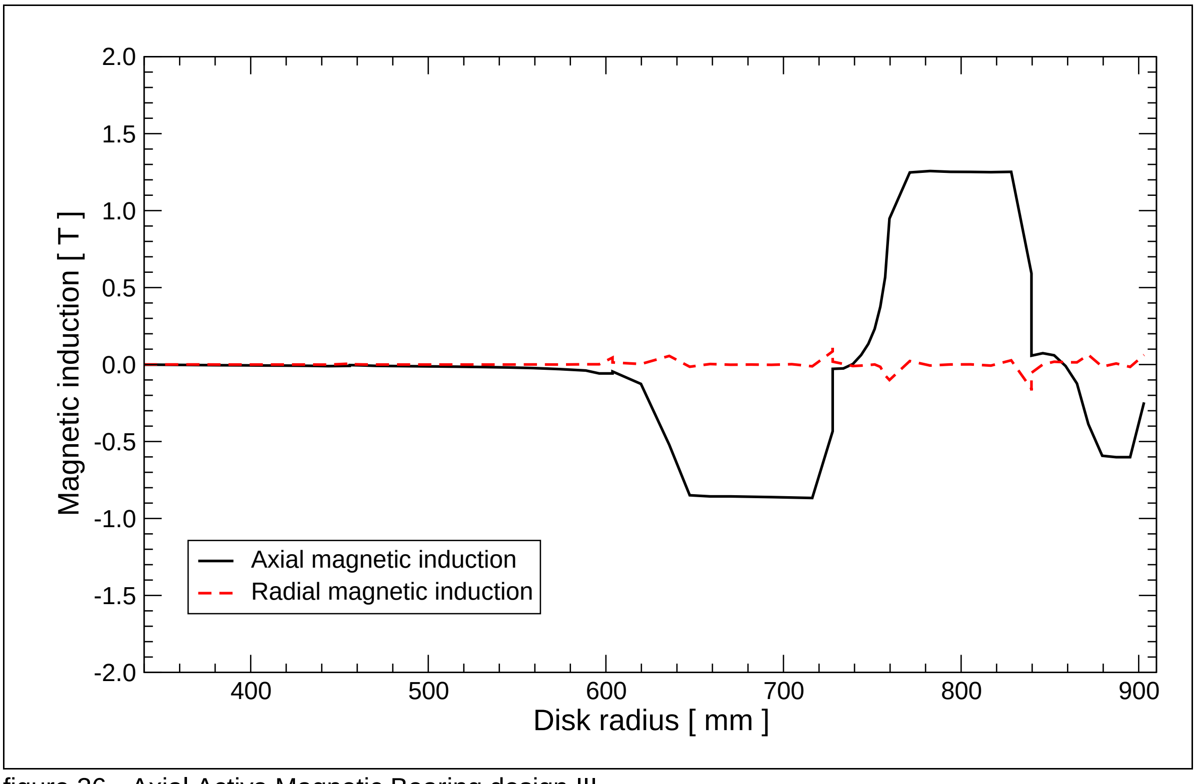


figure 36 Axial Active Magnetic Bearing design III
The magnetic induction in the gap between the stator and the disk (pull mode)

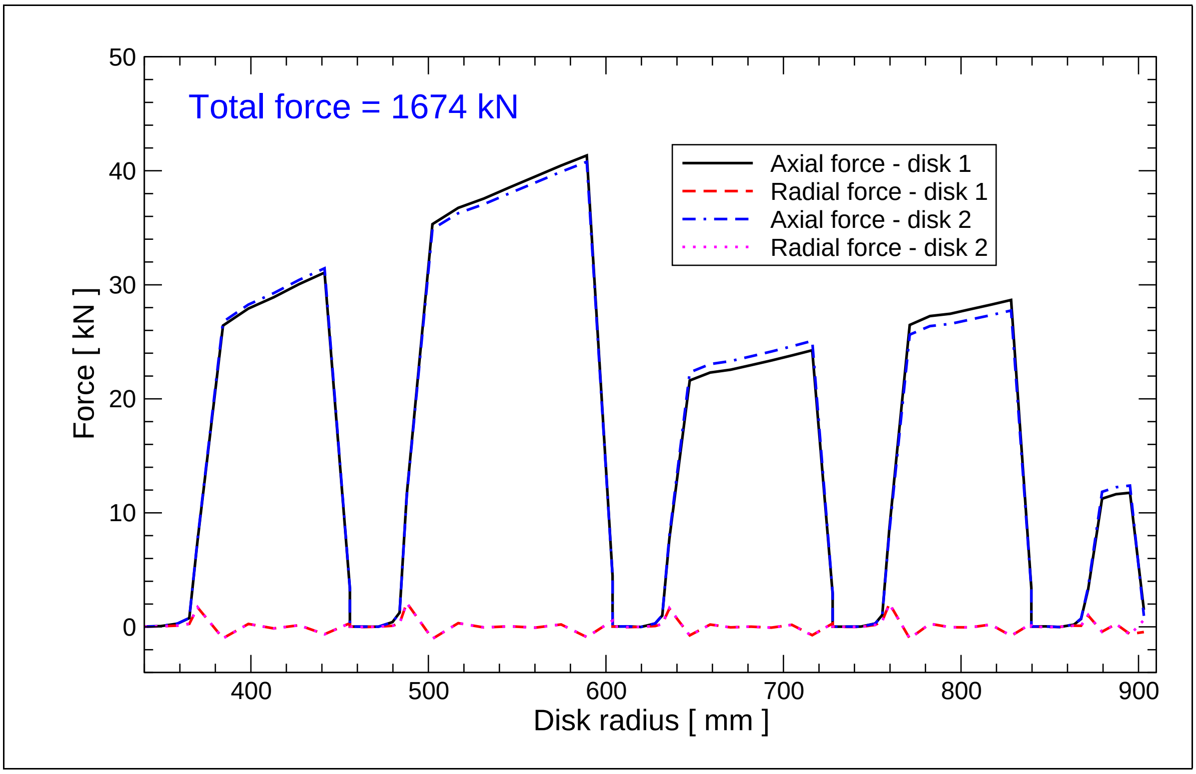


figure 37 Axial Active Magnetic Bearing design III
The magnetic forces on the disk (lift mode)

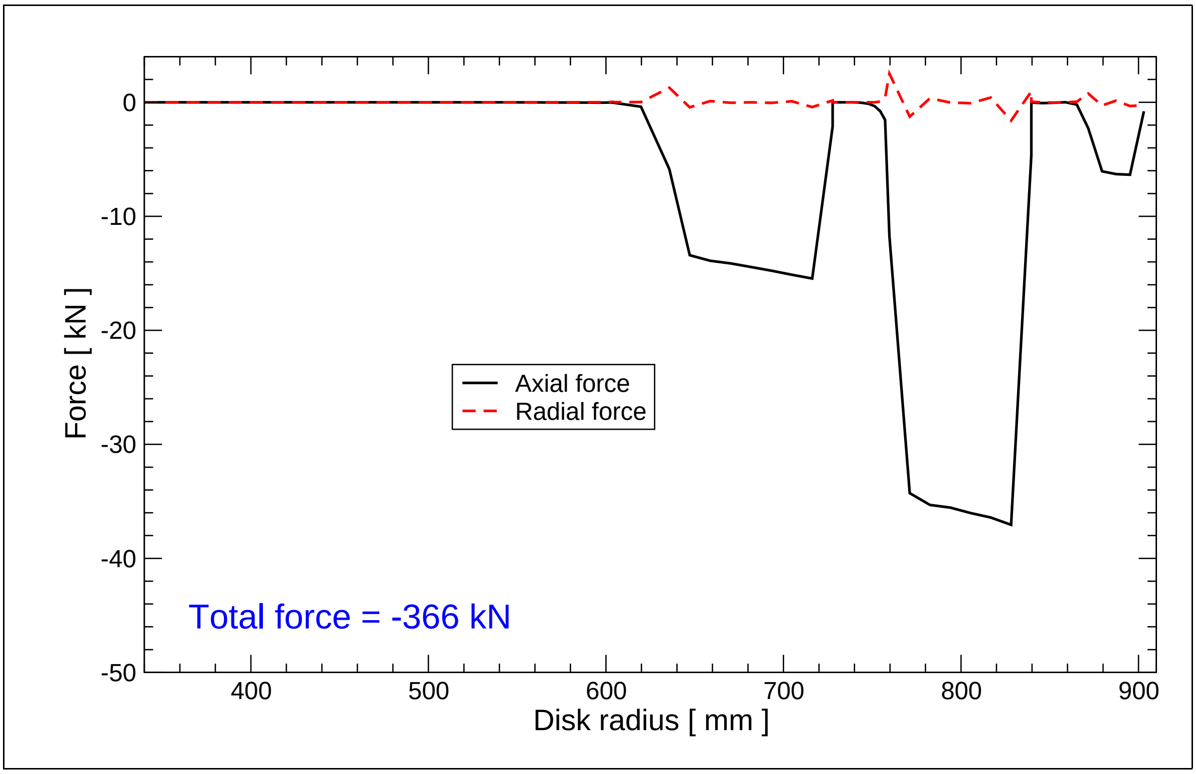


figure 38 Axial Active Magnetic Bearing design III
The magnetic forces on the disk (pull mode)

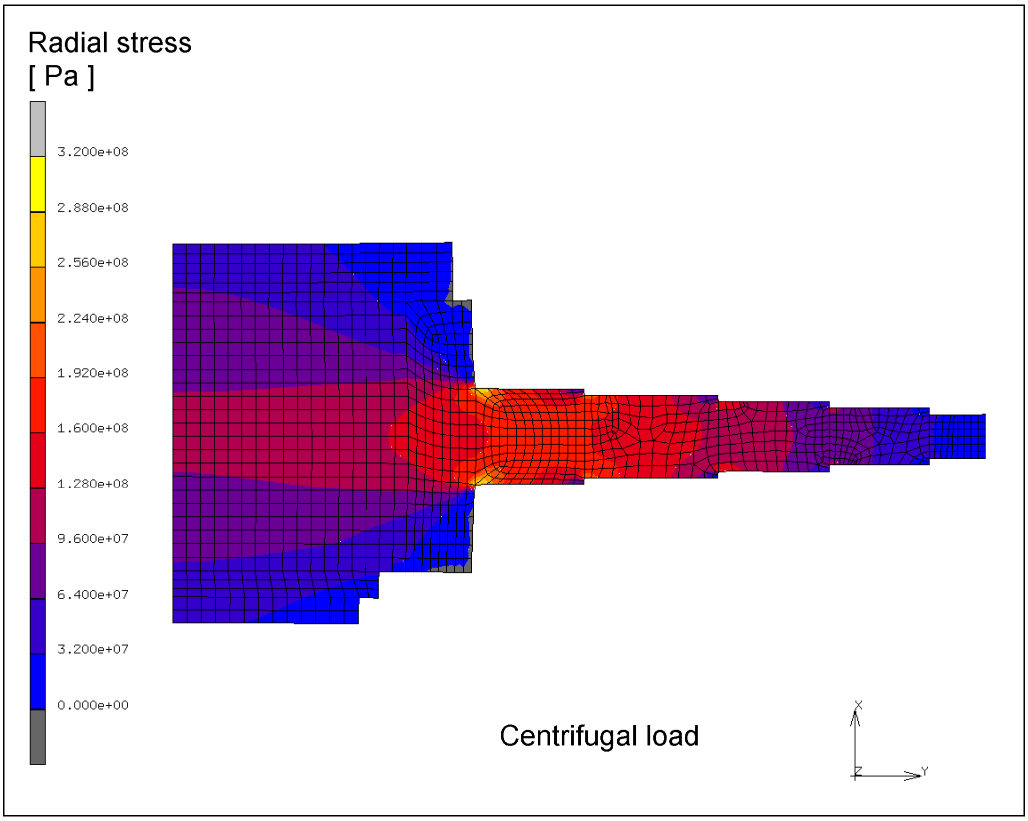


figure 39 Axial Active Magnetic Bearing design
The distribution of the radial stress due to the centrifugal load

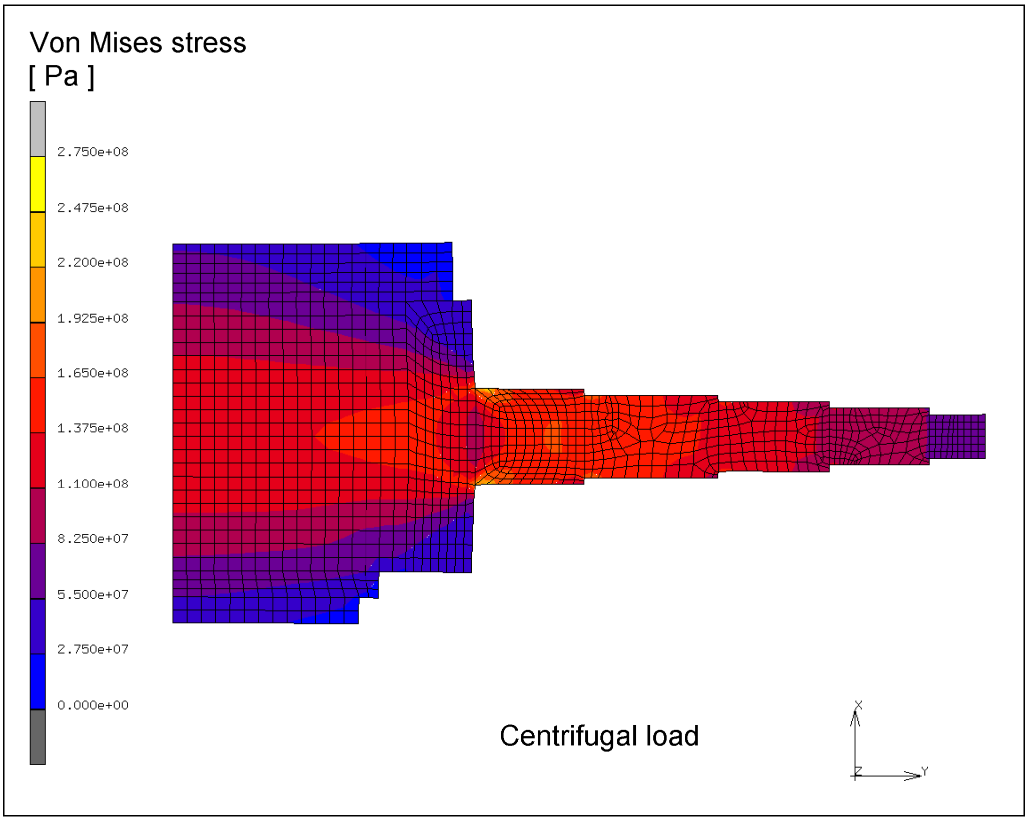


figure 40 Axial Active Magnetic Bearing design
The distribution of the Von Mises stress due to the centrifugal load

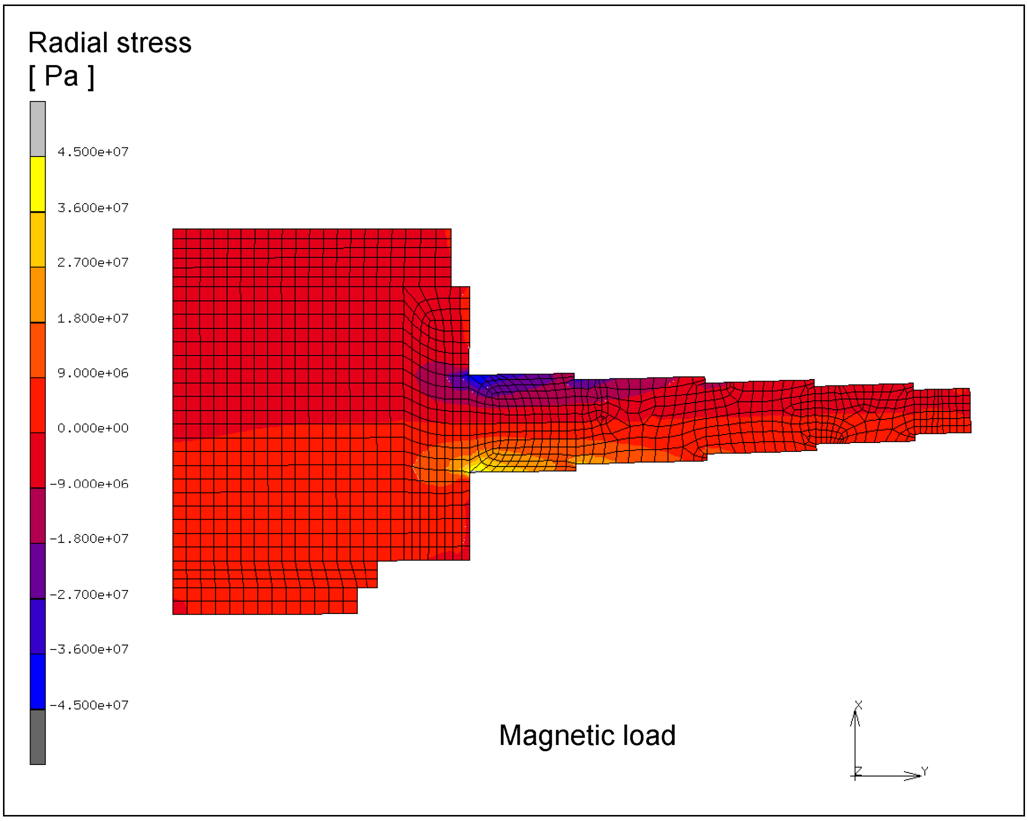


figure 41 Axial Active Magnetic Bearing design
The distribution of the radial stress due to the magnetic load

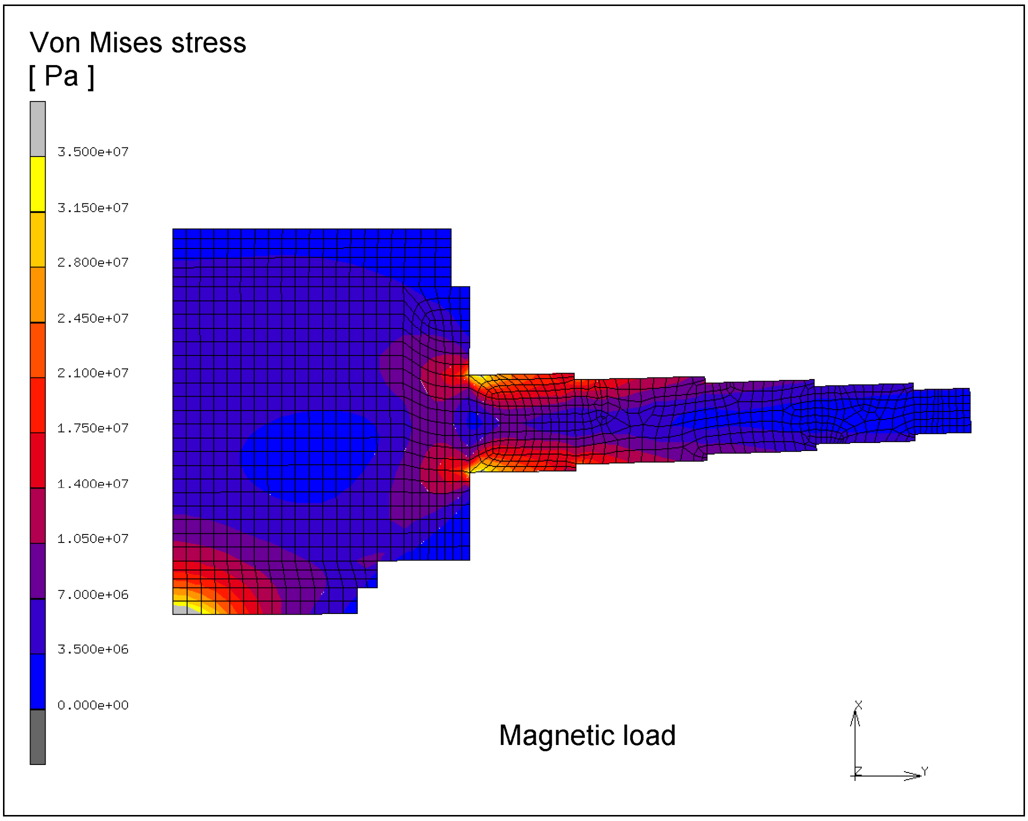


figure 42 Axial Active Magnetic Bearing design
The distribution of the Von Mises stress due to the magnetic load

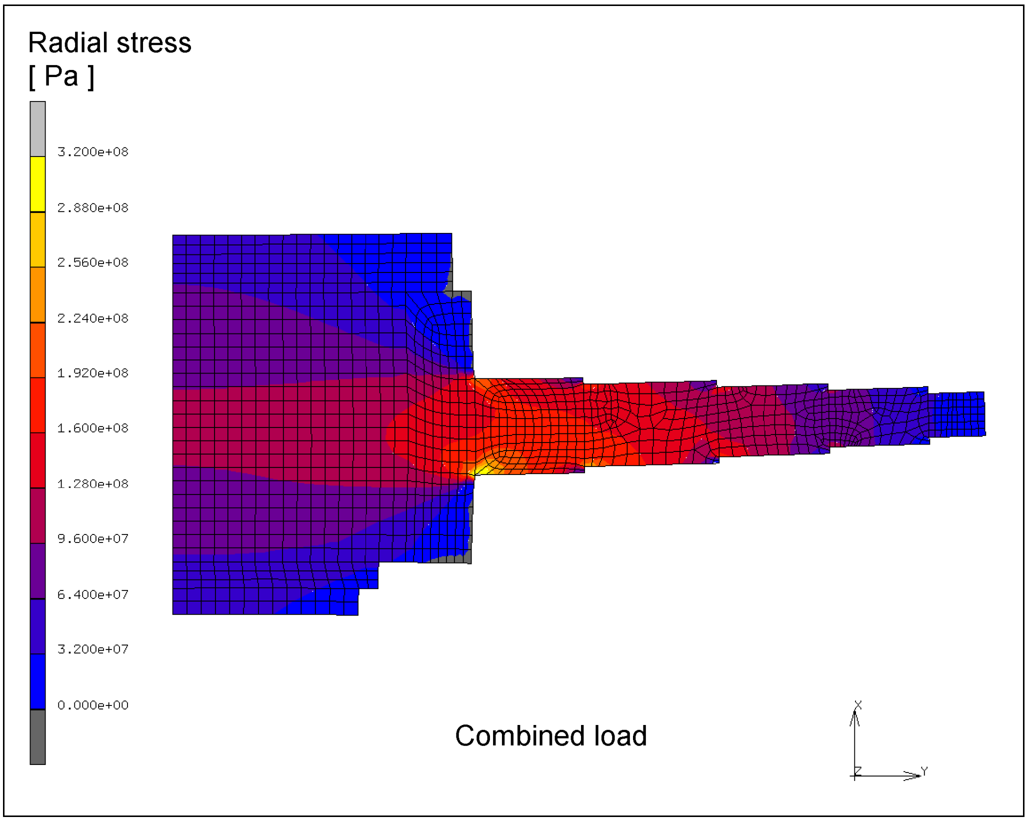


figure 43 Axial Active Magnetic Bearing design
The distribution of the radial stress due to the combined load

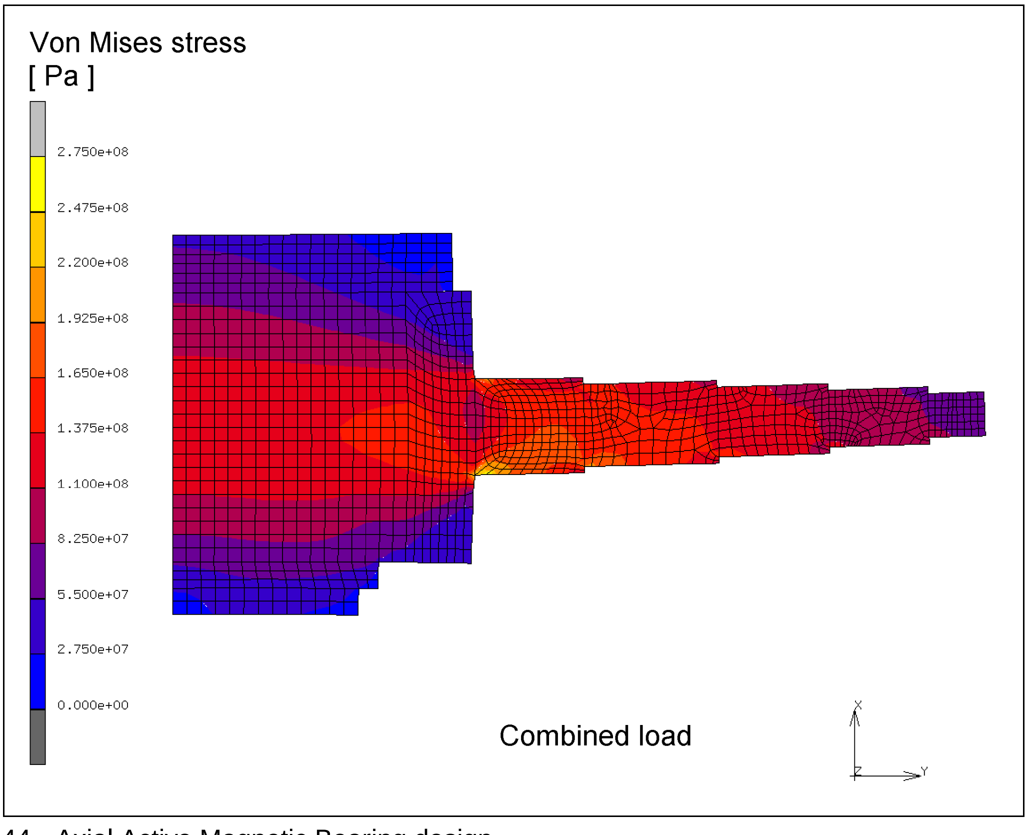


figure 44 Axial Active Magnetic Bearing design
The distribution of the Von Mises stress due to the combined load